

# Scalable particle-based alternatives to EM

Juan Kuntz      Adam M. Johansen

Department of Statistics

University of Warwick

Coventry, CV4 7AL, UK

{juan.kuntz-nussio, a.m.johansen}@warwick.ac.uk

## Abstract

Building on [48], where the problem tackled by EM is recast as the optimization of a free energy functional on an infinite-dimensional space, we obtain three practical particle-based alternatives to EM applicable to broad classes of models. All three are derived through straightforward discretizations of gradient flows associated with the functional. The novel algorithms scale well to high-dimensional settings and outperform existing state-of-the-art methods in numerical experiments.

## 1 Introduction

In machine learning and statistics, we often aim to use a probabilistic model,  $p_\theta(x, y)$ , defined in terms of a vector of parameters,  $\theta$ , to infer some quantities,  $x$ , that we cannot observe experimentally from some,  $y$ , that we can. A pragmatic middleground between Bayesian and frequentist approaches to this type of problem is the *empirical Bayes* (EB) paradigm, dating back to [57], in which we

- (S1) learn the parameters from the data: we search for parameters  $\theta_*$  that explain the data  $y$  well;
- (S2) use  $\theta_*$  to draw inferences on  $x$  with quantified uncertainty.

Because this approach does not require eliciting a prior over the parameters, it is particularly appealing for models with parameters lacking physical interpretations (e.g. the kernel hyperparameters in GP regression) or meaningful prior information. Steps (S1,2) are typically reformulated technically as

- (S1) find a  $\theta_*$  maximizing the *marginal likelihood*  $p_\theta(y) := \int p_\theta(x, y)dx$ ;
- (S2) obtain the corresponding *posterior distribution*  $p_{\theta_*}(x|y) := p_{\theta_*}(x, y)/p_{\theta_*}(y)$ .

Perhaps the most well-known method tackling (S1,2) is the *expectation maximization* (EM) algorithm [22]: starting from an initial guess  $\theta_0$ , alternate,

- (E) compute  $q_{k+1} := p_{\theta_k}(\cdot|y)$ ,
- (M) solve for  $\theta_{k+1} := \arg \max_{\theta \in \Theta} \int \log(p_\theta(x, y))q_{k+1}(dx)$ .

Under general conditions [47, Chap. 3],  $\theta_k$  converges to a stationary point  $\theta_*$  of the marginal likelihood and  $q_k$  to the corresponding posterior  $p_{\theta_*}(\cdot|y)$ . In cases where the above steps are not analytically tractable, it is common to approximate (E) using Monte Carlo (or Markov chain Monte Carlo if  $p_\theta(\cdot|y)$  cannot be sampled directly) and (M) using numerical optimization (e.g. with a single gradient or Newton step in Euclidean spaces); for instance, see [67, 38, 32, 21, 71, 37, 11, 54, 20].

Here, we take a different approach that builds on an insightful observation made by Neal and Hinton twenty-odd years ago [48] (see [17] for a precedent): EM can be recast as a well-known optimization routine applied to a certain objective. The objective is the ‘free energy’ or ‘evidence lower bound’:

$$F(\theta, q) := \int \log \left( \frac{p_\theta(x, y)}{q(x)} \right) q(x) dx = \int \ell(\theta, x) q(x) dx - \int \log(q(x)) q(x) dx \quad (1)$$

for all  $(\theta, q)$  in  $\Theta \times \mathcal{P}(\mathcal{X})$ , where  $\ell(\theta, x) := \log(p_\theta(x, y))$  denotes the log-likelihood,  $\Theta$  the parameter space, and  $\mathcal{P}(\mathcal{X})$  the space of probability distributions on the latent space  $\mathcal{X}$ . The optimization routine is coordinate ascent: starting from an initial guess  $\theta_0$ , alternate,

$$(E) \text{ solve for } q_{k+1} := \arg \max_{q \in \mathcal{P}(\mathcal{X})} F(\theta_k, q), \quad (M) \text{ solve for } \theta_{k+1} := \arg \max_{\theta \in \Theta} F(\theta, q_{k+1}).$$

The key here is the following result associating the maxima of  $p_\theta(y)$  with those of  $F$ :

**Theorem 1.** *For any  $\theta$  in  $\Theta$ , the posterior  $p_\theta(\cdot|y) := p_\theta(\cdot, y)/p_\theta(y)$  maximizes  $q \mapsto F(\theta, q)$ . Moreover,  $p_\theta(y)$  has a global maximum at  $\theta$  if and only if  $F$  has a global maximum at  $(\theta, p_\theta(\cdot|y))$ .*

The theorem follows easily from the same type of arguments as those used to prove [48, Lem. 1, Thrm. 2]. Similar statements can also be made for local maxima, but we refrain from doing so here because it involves specifying what we mean by ‘local’ in  $\Theta \times \mathcal{P}(\mathcal{X})$ . The point is that finding a maximum of  $p_\theta(y)$  and computing the corresponding posterior is equivalent to finding a maximum of  $F$ , and this is precisely what EM does. It has the same drawback as coordinate ascent: we must be able to carry out the coordinate ascent steps (or, equivalently, the EM steps) exactly. Consequently, EM, at least in its original presentation, is limited to relatively simple models.

For more complex models, it is natural to ask: ‘Could we instead solve (S1,2) by applying a different optimization routine to  $F$ ? What about perhaps the most basic of them all, gradient ascent?’. To affirmatively answer both questions, we need (a) a sensible notion of a ‘gradient’ for functionals on  $\Theta \times \mathcal{P}(\mathcal{X})$  and (b) practical methods implementing the gradients steps, at least approximately. At the time of [48]’s publication, these obstacles had already begun to crumble: Otto and coworkers had introduced [35, 50] a notion of gradients for functionals on  $\mathcal{P}(\mathcal{X})$  (w.r.t. to the Wasserstein-2 geometry<sup>1</sup>) and an associated calculus; and [29, 52] had proposed the unadjusted Langevin algorithm (ULA, name coined in [55]) that turned out to be a practical Monte Carlo approximation of the corresponding gradient ascent algorithm applied to a particular functional (although this connection has only been fleshed out much more recently in papers such as [15]). In the ensuing two decades, these two lines of work have progressed greatly: Otto et al.’s ideas has been consolidated and formalized (e.g. [64, 1]), analogues have been established for other geometries on  $\mathcal{P}(\mathcal{X})$  (e.g. [24, 31, 43]), and more practical methods have been published (e.g. [42, 31, 43, 56, 14]).

Here, we capitalize on these developments and obtain scalable easy-to-implement algorithms that tackle (S1,2) for broad classes of models (any for which the density  $p_\theta(x, y)$  is differentiable in  $\theta$  and  $x$ ). We do this in Sec. 2 where we consider three methods: an approximation to gradient ascent (Sec. 2.1), one to Newton’s method (Sec. 2.2), and a further ‘marginal gradient’ method (Sec. 2.3) applicable to models for which the (M) step is tractable but the (E) step is not — a surprisingly common situation in practice. In general, the estimates they produce possess a bias, which we discuss in Sec. 3. We then study their performance in two examples (Sec. 4). We conclude with a discussion of our methods, their limitations, and future research directions (Sec. 5). Interactive Jupyter notebooks, running on Google Colab, that reproduce our plots and tables can be found at <https://github.com/juankuntz/ParEM>.

**Related literature.** Procedures reminiscent of those in Sec. 2 are commonplace in variational inference, e.g. see [36, Sec. 2]. Here, practitioners choose a tractable parametric family  $\mathcal{Q} := (q_\lambda)_{\lambda \in \Lambda} \subseteq \mathcal{P}(\mathcal{X})$ , parametrized by  $\lambda$ s in some set  $\Lambda$ , and solve

$$(\theta_*, \lambda_*) = \arg \max_{(\theta, \lambda) \in \Theta \times \Lambda} F(\theta, q_\lambda) \quad (2)$$

using an appropriate optimization algorithm. If  $\mathcal{Q}$  is sufficiently rich, then  $(\theta_*, q_{\lambda_*})$  will be close to an optimum of  $(\theta, q) \mapsto F(\theta, q)$  if  $(\theta_*, \lambda_*)$  is an optimum of  $(\theta, \lambda) \mapsto F(\theta, q_\lambda)$ . How rich  $\mathcal{Q}$  really needs to be is a complicated question and, in practice,  $\mathcal{Q}$ ’s choice is usually dictated by computational considerations. Because the optimization of interest is that of  $(\theta, q_\lambda)$  over  $\Theta \times \mathcal{Q}$  rather than that of  $(\theta, \lambda)$  over  $\Theta \times \Lambda$ , it often proves beneficial to adapt the optimization routine appropriately. For instance, one could use *natural gradients* (e.g. [46]) defined not w.r.t. the Euclidean geometry on  $\Lambda$  but instead w.r.t. a geometry that accounts for the effect that changes in  $\lambda$  have in  $q_\lambda$ , with changes in  $q_\lambda$  measured by the KL divergence. In this paper, we circumvent these issues by working directly in  $\mathcal{P}(\mathcal{X})$ . We are also guided by similar considerations when choosing  $\theta$  updates (see Secs. 2.2, 2.3 in particular): the object of interest here is the distribution  $p_\theta(\cdot, y)$  indexed by  $\theta$  rather than  $\theta$  itself (but,  $p_\theta(\cdot, y)$  is unnormalized and it is no longer obvious that natural gradients are sensible).

<sup>1</sup>Defining a gradient or ‘direction of maximum ascent’ for a functional on  $\mathcal{P}(\mathcal{X})$  requires quantifying the relative distances of neighbouring points in  $\mathcal{P}(\mathcal{X})$  and, consequently, a metric. Otto et al.’s original work used the Wasserstein-2 metric on  $\mathcal{P}(\mathcal{X})$ , hence the ‘Wasserstein-2 geometry’ jargon. For more on this, see App. A.

Well-known algorithms are recovered as ‘corner cases’ of ours. For example, if the parameter space is trivial ( $\Theta = \{\theta\}$ ) and we use a single particle ( $N = 1$  in what follows), the methods in Sec. 2 reduce to ULA [55] applied to the unnormalized density  $p_\theta(\cdot, y)$ . If, on the other hand, the latent space is trivial, the algorithm in Sec. 2.1 collapses to gradient ascent applied to  $\theta \mapsto p_\theta(y)$  and that in Sec. 2.2 to Newton’s method. Lastly, although we find the empirical Bayes setting a natural one for introducing our methods, the EM algorithm can also be used to tackle many other problems (e.g. see [47, Chap. 8]) and, subject to the limitations discussed in Sec. 5, so can ours.

**Our setting, notation, assumptions, rigour, and lack thereof.** In this methodological paper we favour intuition and clarity of presentation over mathematical rigour. We believe that all of the statements we make can be argued rigorously under the appropriate technical conditions, but we do not dwell on what these are. Except where strictly necessary, we avoid measure-theoretic notation and we commit the usual notational abuse of conflating measures and kernels with their densities w.r.t. to the Lebesgue measure (this can be remedied by interpreting equations weakly and replacing density ratios with Radon-Nikodym derivatives). We also focus on Euclidean parameter and latent spaces ( $\Theta = \mathbb{R}^{D_\theta}$  and  $\mathcal{X} = \mathbb{R}^{D_x}$  for  $D_\theta, D_x > 0$ ), although our results and methods apply almost unchanged were these to be differentiable Riemannian manifolds. Throughout,  $\mathbf{1}_d$  and  $I_d$  respectively denote the  $d$ -dimensional vector of ones and identity matrix,  $\mathcal{N}(\mu, \Sigma)$  the normal distribution with mean vector  $\mu$  and covariance matrix  $\Sigma$ , and  $\mathcal{N}(x; \mu, \Sigma)$  its density evaluated at  $x$ . We also tacitly assume that  $p_\theta(x, y) > 0$  for all  $\theta, x$ , and  $y$ ; and that  $(\theta, x) \mapsto p_\theta(x, y)$  is sufficiently regular that any gradients or Hessians we use are well-defined and any integral-derivatives swaps and applications of integration-by-parts we use are justified. Furthermore, we make the following assumption, the violation of which indicates a poorly parametrized model or insufficiently informative data.

**Assumption 1.** *The marginal likelihood’s super-level sets  $\{\theta \in \Theta : p_\theta(y) \geq l\}$  are bounded.*

## 2 Three algorithms

### 2.1 The particle gradient ascent (PGA) algorithm

Recall that the basic gradient ascent algorithm for maximizing a differentiable function  $f : \mathbb{R}^n \rightarrow \mathbb{R}$ ,

$$x_{k+1} = x_k + h \nabla_x f(x_k), \quad (3)$$

is the Euler discretization with step size  $h > 0$  of  $f$ ’s continuous-time *gradient flow*  $\dot{x}_t = \nabla_x f(x_t)$ , where  $\nabla_x$  denotes the usual Euclidean gradient w.r.t. to  $x$ . To obtain an appropriate analogue of (3) applicable to  $F$  in (1), we identify an analogue of  $f$ ’s gradient flow and discretize it. Here, we require a sensible notion for  $F$ ’s gradient. We use  $\nabla F(\theta, q) = (\nabla_\theta F(\theta, q), \nabla_q F(\theta, q))$ , where

$$\nabla_\theta F(\theta, q) = \int \nabla_\theta \ell(\theta, x) q(x) dx, \quad \nabla_q F(\theta, q) = -\nabla_x \cdot \left[ q \nabla_x \log \left( \frac{p_\theta(\cdot, y)}{q} \right) \right]. \quad (4)$$

This is the gradient obtained if we endow  $\Theta$  with the Euclidean geometry and  $\mathcal{P}(\mathcal{X})$  with the Wasserstein-2 one (see App. B.1). It vanishes if and only if  $\theta$  is a stationary point of the marginal likelihood and  $q$  is its corresponding posterior:

**Theorem 2** ( $1^{st}$  order optimality condition).  $\nabla F(\theta, q) = 0$  iff  $\nabla_\theta p_\theta(y) = 0$  and  $q = p_\theta(\cdot|y)$ .

See App. C for a proof. The corresponding gradient flow reads

$$\dot{\theta}_t = \int \nabla_\theta \ell(\theta_t, x) q_t(x) dx, \quad \dot{q}_t = -\nabla_x \cdot \left[ q_t \nabla_x \log \left( \frac{p_{\theta_t}(\cdot, y)}{q_t} \right) \right]. \quad (5)$$

Given Assumpt. 1 and Thrm. 2, we expect that an extension of LaSalle’s principle [12, Thrm. 1] will show that, as  $t$  tends to infinity,  $\theta_t$  approaches a stationary point  $\theta_*$  of  $\theta \mapsto p_\theta(y)$  and  $q_t$  the corresponding posterior  $p_{\theta_*}(\cdot|y)$ ; see App. D for more on this and a proof in a special case.

Eq. (5) can rarely be solved analytically. To overcome this, note that it is a mean-field Fokker-Planck equation satisfied by the law of the following McKean-Vlasov SDE (e.g. [13, Sec. 2.2.2]):

$$d\theta_t = \left[ \int \nabla_{\theta} \ell(\theta_t, x) q_t(x) dx \right] dt, \quad dX_t = \nabla_x \ell(\theta_t, X_t) dt + \sqrt{2} dW_t, \quad (6)$$

where  $q_t$  denotes  $X_t$ 's law and  $(W_t)_{t \geq 0}$  a standard  $D_x$ -dimensional Brownian motion. To obtain an implementable algorithm we now require a tractable approximation to the integral in (6) and a discretization of the time axis. For the former, we use a finite-sample approximation to  $q_t$ : we generate  $N > 0$  particles  $X_t^1, \dots, X_t^N$  with law  $q_t$  by solving

$$dX_t^n = \nabla_x \ell(\theta_t, X_t^n) dt + \sqrt{2} dW_t^n \quad \forall n \in [N] := \{1, \dots, N\}, \quad (7)$$

with  $(W_t^1)_{t \geq 0}, \dots, (W_t^N)_{t \geq 0}$  denoting  $N$  independent Brownian motions, and exploit

$$q_t \approx \frac{1}{N} \sum_{n=1}^N \delta_{X_t^n} \Rightarrow \int \nabla_{\theta} \ell(\theta_t, x) q_t(x) dx \approx \frac{1}{N} \sum_{n=1}^N \nabla_{\theta} \ell(\theta_t, X_t^n), \quad (8)$$

where  $\delta_x$  denotes a Dirac delta at  $x$ . We then obtain the following approximation to (6LHS,7):

$$d\theta_t = \left[ \frac{1}{N} \sum_{n=1}^N \nabla_{\theta} \ell(\theta_t, X_t^n) \right] dt, \quad dX_t^n = \nabla_x \ell(\theta_t, X_t^n) dt + \sqrt{2} dW_t^n \quad \forall n \in [N].$$

Discretizing the above using the Euler-Maruyama scheme, we obtain an implementable particle-based approximation to (5) given by  $(\theta_k, q_k := N^{-1} \sum_{n=1}^N \delta_{X_k^n})_{k=1}^K$ , where

$$\theta_{k+1} = \theta_k + \frac{h}{N} \sum_{n=1}^N \nabla_{\theta} \ell(\theta_k, X_k^n), \quad X_{k+1}^n = X_k^n + h \nabla_x \ell(\theta_k, X_k^n) + \sqrt{2h} W_k^n \quad \forall n \in [N], \quad (9)$$

for all  $k$  in  $[K]$ , with  $K > 0$  denoting the number of steps,  $h > 0$  the step size, and  $(W_k^n)_{k \in [K-1], n \in [N]}$  independent standard normal random variables. We then estimate a stationary point  $\theta_*$  of the marginal likelihood  $\theta \mapsto p_{\theta}(y)$  and its corresponding posterior  $p_{\theta_*}(\cdot|y)$  using

$$\theta_K, q_K \quad \text{or} \quad \bar{\theta}_K := \frac{1}{(K - k_b)} \sum_{k=k_b+1}^K \theta_k, \quad \bar{q}_K := \frac{1}{(K - k_b)} \sum_{k=k_b+1}^K q_k, \quad (10)$$

where  $k_b < K$  denotes the number of steps that we discard during burn-in. Given the analogy between (3) and (9), we formulate conjectures for  $(\theta_k, q_k)$ 's behaviour based on our understanding of (stochastic) gradient ascent (note that (9) involves noisy estimates of  $F$ 's gradient) and Thrm. 2:

- (C1) If the step size  $h$  is set too large, (9) will be unstable.
- (C2) Otherwise, after a transient phase,  $\theta_k$  will hover around a stationary point  $\theta_*$  of  $\theta \mapsto p_{\theta}(y)$ ,  $q_k$  around the corresponding posterior  $p_{\theta_*}(\cdot|y)$ , and  $(\bar{\theta}_k, \bar{q}_k)$  will converge to  $(\theta_*, p_{\theta_*}(\cdot|y))$ .
- (C3) Small  $h$ s lead to long transient phases but low estimator variance in the stationary phase.

Modulo the bias we discuss in Sec. 3, the above is what we observe in practice:

**Example 1.** Consider the toy hierarchical model involving a single scalar unknown parameter  $\theta$ ,  $D_x$  i.i.d. mean- $\theta$  unit-variance Gaussian latent variables, and, for each of these, an independent observed variable with unit-variance Gaussian law centred at the latent variable:

$$p_{\theta}(x, y) := \prod_{d=1}^{D_x} \frac{1}{2\pi} \exp \left( -\frac{(x_d - \theta)^2}{2} - \frac{(y_d - x_d)^2}{2} \right) \quad \forall \theta \in \mathbb{R}, \quad x, y \in \mathbb{R}^{D_x}. \quad (11)$$

It is straightforward to verify that the marginal likelihood  $\theta \mapsto p_{\theta}(y)$  has a unique maxima,  $\theta_* = D_x^{-1} \sum_{d=1}^{D_x} y_d$ , and obtain expressions for the corresponding posterior (see App. F.1). Running (9) we find the following: if the step size  $h$  is chosen too large,  $\theta_k$  is unstable (1a, grey). If  $h$  is chosen well,  $\theta_k$  approaches  $\theta_*$  and hovers around it (1a, black solid) in such a way  $\bar{\theta}_k$  converges to it (1b, blue line). If  $h$  is chosen too small, the convergence is slow (1a, black dashed).

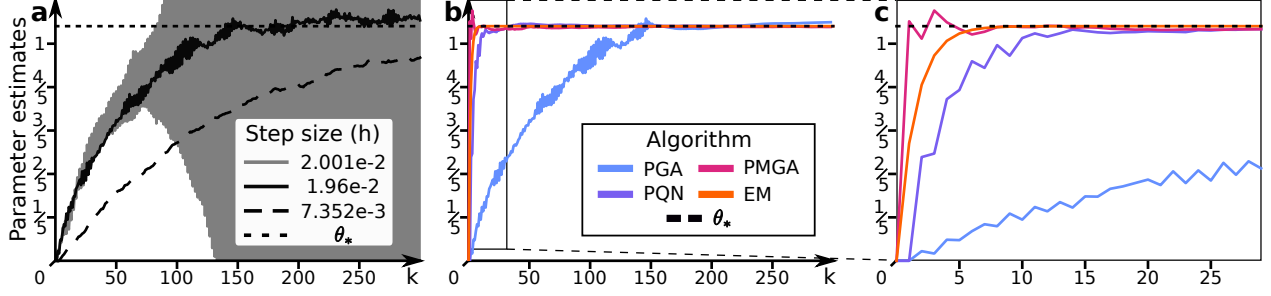


Figure 1: **Toy hierarchical model.** Parameter estimates for Ex. 1 with  $D_x = 100$  latent variables,  $N = 10$  particles, and both particles and estimates initialized at zero. **a** PGA estimates  $\theta_k$  for three step sizes  $h$ . **b** PGA, PQN, PMGA, and EM parameter estimates. EM converges without averaging over time. For PGA, PQN, and PMGA we use optimal step sizes (respectively,  $h = 1/51, 2/3, 1$ , cf. App. G.1) and start averaging once the estimates reach stationarity (i.e. plot shows  $\theta_k$  for  $k < k_b$  and  $\theta_k$  for  $k \geq k_b$  with  $k_b = 150, 15, 5$  for PGA, PQN, PMGA, respectively). **c** First 30 steps in b.

**Separation of time-scales and a simple heuristic fix.** For many models, each component of  $\nabla_\theta \ell(\theta, x)$  is a sum of  $D \gg 1$  terms and, consequently, takes large values. On other hand, each component of  $\nabla_x \ell(\theta, x)$  typically involves far fewer terms (for instance, two in Ex. 1 while  $D = D_x$ ). Hence, (9) often ends up taking much larger steps in the  $\theta$ -coordinates than in the  $x$ -coordinates. This ‘separation of time-scales’ causes (9) to have poor numerical properties. In particular, it forces us to employ small step sizes  $h$  in order to keep  $\theta_k$  stable. This results in ‘poor mixing’ for the  $x$ -coordinates and overall slow convergence. In our experiments, we found that a simple heuristic significantly mitigates the issue: in the  $\theta$  update, divide each component of  $\nabla_\theta \ell(\theta, x)$  by the corresponding number of terms ( $D_x$  in Ex. 1, see Sec. 4.2 for another example). Note that this amounts to pre-multiplying  $\nabla_\theta \ell(\theta, x)$  in (9) by positive definite matrix  $\Lambda$  and, hence, does not alter (9)’s fixed points. That is, we replace (9LHS) with

$$\theta_{k+1} = \theta_k + \frac{h}{N} \sum_{n=1}^N \Lambda \nabla_\theta \ell(\theta_k, X_k^n). \quad (12)$$

For some simple models, (9RHS,12) coincides with the quasi-Newton method discussed in Sec. 2.2; in more complicated ones, it can be viewed as a crude approximation thereof.

## 2.2 The particle quasi-Newton (PQN) algorithm

A slightly more elaborate variant of (9) that also seems to resolve the time-scale issue and, furthermore, achieve faster convergence entails replacing (9LHS) with

$$\theta_{k+1} = \theta_k + h \left[ \sum_{n=1}^N \mathcal{H}_\theta(X_k^n) \right]^{-1} \sum_{n=1}^N \nabla_\theta \ell(\theta_k, X_k^n) \quad \text{with} \quad \mathcal{H}_\theta(x) := - \left( \frac{\partial^2 \ell(\theta, x)}{\partial \theta_i \partial \theta_j} \right)_{ij}. \quad (13)$$

(We assume that the log-likelihood’s negative  $\theta$ -Hessian,  $\mathcal{H}_\theta(x)$ , is full-rank for all  $(\theta, x)$  in  $\Theta \times \mathcal{X}$ .) Here, we also use (10) to obtain estimates of the marginal likelihood’s stationary points and their associated posteriors. (9RHS,13) arises as a discretization (similar to that in Sec. 2.1) of

$$\dot{\theta}_t = \left[ \int \mathcal{H}_{\theta_t}(x) q_t(x) dx \right]^{-1} \int \nabla_\theta \ell(\theta_t, x) q_t(x) dx, \quad \dot{q}_t = -\nabla_x \cdot \left[ q_t \nabla_x \log \left( \frac{p_{\theta_t}(\cdot, y)}{q_t} \right) \right], \quad (14)$$

which itself is an approximation to  $F$ ’s Newton flow (analogous to the gradient flow except that we follow the Newton direction rather than the gradient), see Apps. B.2, E.1. Our full-rank assumption implies that (14)’s fixed points are  $F$ ’s stationary points, and Thrm. 2 applies as before.

At first glance, (13) mitigates the time-scale issue for the same reason that (12) does:  $\mathcal{H}_\theta(x)$ 's entries generally have a similar number of terms to  $\nabla_\theta \ell(\theta, x)$ 's, which prevents excessively large  $\theta$ -updates. In fact, for the toy model in Ex. 1,  $\mathcal{H}_\theta \equiv \Lambda^{-1} = D_x$  and (12,13) coincide. A bit less superficially, this might be because the RHS of the equations in (14) form an approximation to  $F$ 's Newton direction at  $(\theta_t, q_t)$  and, hence, better account for the effect that the updates have on  $F$ 's value. This is also the reason why we believe that (9RHS,13) often converges faster than (9), e.g. see Fig. 1b and App. G.1. The price to pay, of course, is the extra cost incurred by the Hessian evaluations and the matrix inversion in (13). But, for many models  $D_x \gg D_\theta$  (for instance, those in Ex. 1 and Sec. 4.2), and this overhead is small compared with the cost of the  $x$ -updates.

## 2.3 The particle marginal gradient ascent (PMGA) algorithm

For a surprising number of models in the literature, the (M) step is tractable. In particular:

**Assumption 2.** *For each  $q$  in  $\mathcal{P}(\mathcal{X})$ ,  $\theta \mapsto F(\theta, q)$  has a unique stationary point  $\theta_*(q)$ .*

Moreover, we are able to compute this point  $\theta_*(x^{1:N}) := \theta_*(q)$  whenever  $q = N^{-1} \sum_{n=1}^N \delta_{x^n}$  for  $x^{1:N} = (x^1, \dots, x^N)$  in  $\mathcal{X}^N$ . In these cases, we can run the ‘marginal gradient ascent’ algorithm,

$$X_{k+1}^n = X_k^n + h \nabla_x \ell(\theta_*(X_k^{1:N}), X_k^n) + \sqrt{2h} W_k^n \quad \forall n \in [N] \quad (15)$$

where  $(W_k^n)_{k \in [K-1], n \in [N]}$  again denotes a collection of independent standard normal R.V.s, and we also use analogues of (10) to estimate  $\theta_*$  and  $p_{\theta_*}(\cdot|y)$ . For the reasons given in App. E.2, the above is an approximation to Wasserstein-2 gradient flow of the ‘marginal objective’  $F_*(q) := F(\theta_*(q), q)$ :

$$\dot{q}_t = \nabla F_*(q_t), \quad \text{where} \quad \nabla F_*(q) = -\nabla_x \cdot \left[ q \nabla_x \log \left( \frac{p_{\theta_*(q)}(\cdot, y)}{q} \right) \right]. \quad (16)$$

Thrm. 2 is easily adapted to this setting, see App. C for a proof.

**Theorem 3.**  *$\theta = \theta_*(q)$  and  $\nabla F_*(q) = 0$  if and only if  $\nabla_\theta p_\theta(y) = 0$  and  $q = p_\theta(\cdot|y)$ .*

Exploiting the availability of  $\theta_*(q)$  seems to improve the convergence. For example, see Fig. 1b,c (in fact, for this simple model, it is straightforward to find theoretical evidence supporting this, cf. App. G.1). Lastly, we point out that in cases where  $\theta_*(x^{1:N})$  is not analytically tractable, but  $D_\theta$  is small (at least in comparison to  $D_x$ ), we can instead approximately compute  $\theta_*(X_k^{1:N})$  using an appropriate optimization routine (warm-starting  $\theta_*(X_k^{1:N})$ 's computation using  $\theta_*(X_{k-1}^{1:N})$ ).

## 3 The bias

For all three algorithms in Sec. 2, (C2) in Sec. 2.1 does not quite hold true: the estimates produced by the algorithms are biased in the sense that the of  $(\bar{\theta}_k, \bar{q}_k)$  does not converge exactly to  $(\theta_*, p_{\theta_*}(\cdot|y))$ , but rather to a point in its vicinity. The bias stems from two sources:

- (B1)  $h > 0$ . Euler-Maruyama discretizations of the Langevin diffusion do not preserve stationary distributions: this can be seen by examining mean field limits of (9,13,15), cf. App. G.
- (B2)  $N < \infty$ . Our use of finite particle populations: this is best understood by studying continuum limits of (9,13,15), cf. App. H.

B1 can be mitigated by decreasing the step size and B2 by increasing the particle number:

**Example 2.** *Consider again Ex. 1. In this simple case, (B1,2) do not materialize in the  $\theta$ -estimates (Fig. 1) because the model ‘is linear in  $\theta$ ’, cf. App. H.1. To observe (B1,2) we must examine the model’s ‘non-linear aspects’, for instance the posterior variance whose estimates are biased (Fig. 2).*

Of course, increasing  $N$  grows the algorithm’s cost and excessively lowering  $h$  slows its convergence. However, computations across particles are easily vectorized which substantially mitigates the cost growth (cf. Sec. 4). It seems also to be possible to eliminate B1 altogether by adding population-wide accept-reject steps as described in App. I, see Fig. 2c. However, we do not dwell on this type of approach because its scalability is limited by a practical downside: the acceptance probability degenerates for large  $D_x$  and  $N$ , forcing small choices of  $h$  and slow convergence.



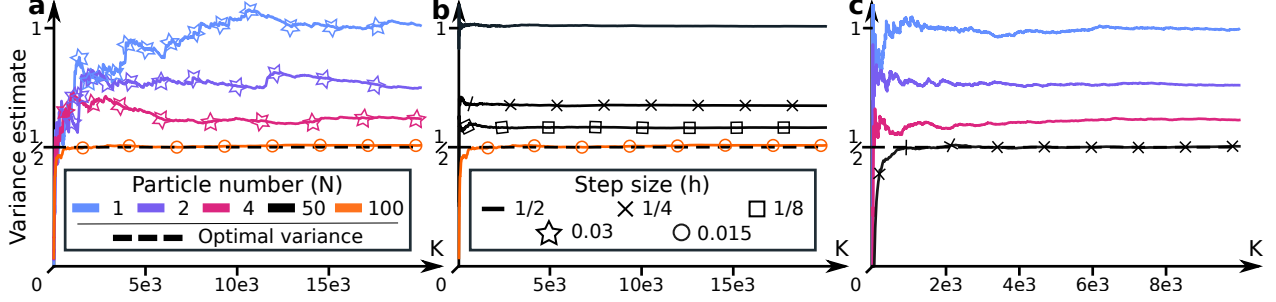


Figure 2: **Toy hierarchical model, bias.** PMGA estimates for the posterior variance in the  $D_x = 1$  case using the time-averaged posterior approximation  $\bar{q}_K$  and no burn-in ( $k_b = 0$ ), as a function of  $K$ . (a) Even with a small step size  $h$ , using a single particle leads to a significant bias (blue). Growing the particle number  $N$  reduces the bias (purple, magenta). The bias becomes negligible for small  $h$  and large  $N$  (orange). (b) Even with large  $N$ , large  $h$  lead to significant bias (solid). Decreasing  $h$  reduces the bias (crosses, squares, circles). (c) Adding an accept-reject step removes (B1) regardless of the  $h$  employed, and the remaining bias can be removed by choosing a sufficiently large  $N$ .

## 4 Numerical experiments

We illustrate the application of our methods and examine their performance via two classification tasks: Bayesian logistic regression applied to the Wisconsin Breast Cancer dataset (Sec. 4.1) and a simple Bayesian neural network applied to the MNIST dataset (Sec. 4.2). We implement the methods in Python 3 and JAX [9], and we carry out all experiments using a Tesla K80 GPU. We benchmark using the Stochastic Optimisation via Unadjusted Langevin (SOUL) algorithm<sup>2</sup>, recently proposed [20] to overcome the limited scalability of traditional MCMC EM variants. Because it is a coordinate-wise cousin of PGA (Sec. 2.1), it allows for straightforward meaningful comparisons with our methods. It approximates the (M) step by updating the parameter estimates using a single (stochastic) gradient step as we do in (9LHS). For the (E) step, it instead runs a single ULA chain for  $N$  steps, ‘warm-started’ using the previous chain’s final state ( $X_{k+1}^1 := X_k^N$ ):

$$X_{k+1}^{n+1} = X_{k+1}^n + h \nabla_x \ell(\theta_k, X_{k+1}^n) + \sqrt{2h} W_{k+1}^n \quad \forall n \in [N-1]; \quad (17)$$

and then approximates  $p_{\theta_{k+1}}(\cdot|y)$  using the chain’s empirical distribution  $q_{k+1} := N^{-1} \sum_{n=1}^N \delta_{X_{k+1}^n}$ .

### 4.1 Bayesian logistic regression

We consider the set-up described in [20, Sec. 4.1] and employ the same dataset with 683 datapoints, cf. App. F.2 for details. The latent variables are the 9 regression weights. We assign an isotropic Gaussian prior  $\mathcal{N}(\theta \mathbf{1}_{D_x}, 5I_{D_x})$  to the weights and learn the scalar parameter  $\theta$  from the data (i.e. we estimate the marginal likelihood’s unique maximizer  $\theta_*$ , cf. Prop. 1 in App. F.2 for the uniqueness).

The parameter estimates produced by all four algorithms converge to the same limit (Fig. 3a). SOUL is known [20] to return accurate estimates of  $\theta_*$  for this example, so we presume that this limit approximately equals  $\theta_*$ . All algorithms produce posterior approximations with similar predictive power regardless of the particle number  $N$  (Tab. 2 in App. F.2): the task is simple and it is straightforward to achieve good performance. In particular, the posteriors are unimodal and peaked (e.g. see [20, Fig. 2]) and approximated well using a single particle in the vicinity of their modes.

We found three noteworthy differences between SOUL and our methods. First, the computations in (9RHS, 15) are easily vectorized across particles while those in (17) must be done in serial. This results in our algorithms running substantially faster, with the gap in computation times growing with  $N$  (Tab. 2). Second, SOUL tends to produce more peaked posterior approximations than our methods (Fig. 3b), which is not surprising given that particles  $X_{k+1}^1, \dots, X_{k+1}^N$  in (17) are strongly sequentially correlated, while those in

<sup>2</sup>In [20] the authors allow for step sizes and particle number that change with  $k$ . To simplify the comparison and place all methods in equal footing, we fix a single step size  $h$  and particle number  $N$ .

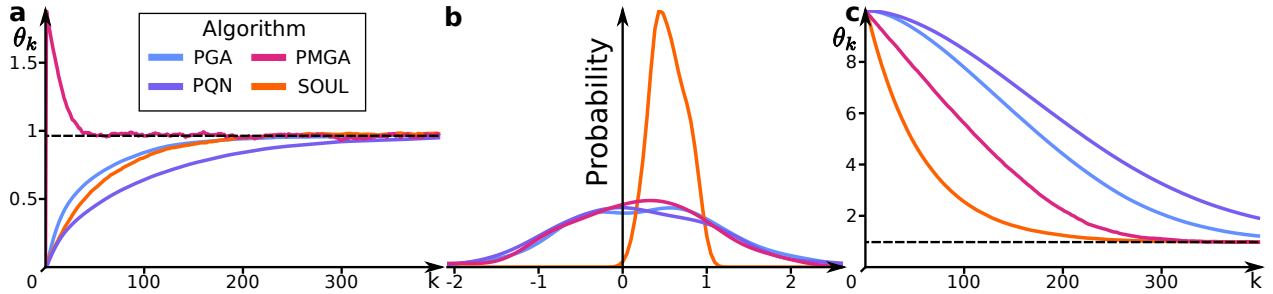


Figure 3: **Bayesian logistic regression.** **a** Parameter estimates  $\theta_k$  as a function of  $k$  with  $N = 100$  particles and a step size of  $h = 0.01$ , initialized as in [20] (particles and estimates at zero). **b** KDE of the second entry of  $X_{400}^{1:100}$ . **c** As in a, but with particles and estimates initialized at ten.

(9RHS,15) are only weakly correlated through the (mean-field)  $\theta$ -estimates. Last, if the parameter estimates are initialized far from  $\theta_*$  and the particles are initialized far from  $p_{\theta_*}(\cdot|y)$ 's mode, then SOUL exhibits a shorter transient than our algorithms (Fig. 3c). This is because SOUL updates a single particle  $N$  times per parameter update and quickly locates the current posteriors' mode, while our algorithms are stuck slowly moving  $N$  particles, one update per  $\theta$ -update, to the posteriors's mode. However, in this example, we found little benefit in using any method with more than one particle, at least until the transient phase was over. To obtain good predictive performance, we found it most expedient to use any method with a single particle; to obtain low variance estimates of  $\theta_*$ , we found it most efficient to use any algorithm with  $N = 1$  during the transient phase before moving to PGA or PQN with computations vectorized across particles (Tab. 2).

## 4.2 Bayesian neural network

To test our methods on a more challenging example, we turn to Bayesian neural networks whose posteriors are notoriously multimodal. In particular, we consider the same setting as in [70, Sec. 6.5] and apply a simple two-layer neural network to the MNIST classification task, cf. App. F.3 for details. Similarly to [70], we avoid any big data issues by subsampling 1000 data points with labels 4, 9. The input layer has 40 nodes and 784 inputs, the output layer has 2 nodes. The latent variables are the weights,  $w \in \mathbb{R}^{40 \times 784}$ , of the input layer and those,  $v \in \mathbb{R}^{2 \times 40}$ , of the output layer. As in [70], we assign zero-mean isotropic Gaussian priors to the weights with respective variances  $e^{2\alpha}$  and  $e^{2\beta}$ . However, rather than assigning a hyperprior to  $\alpha, \beta$ , we instead learn them from the data (i.e.  $\theta := (\alpha, \beta)$ ). To avoid any memory issues, we only store the current particle cloud and use its empirical distribution to approximate the posteriors (rather than a time-averaged version thereof).

All four algorithms exhibit a short transient in their parameter estimates and predictive performances, after which the estimates appear to converge to different local maxima of the marginal likelihood (Fig. 4a) and the performances of PGA, PQN, and PMGA show a slow moderate increase (Fig. 4c). SOUL achieves noticeably worse predictive performance than PGA, PQN, and PMGA (Fig 4c) and shows little improvement with larger particle numbers  $N$  (Tab. 1). We believe that this is due to the peaked SOUL posterior approximations (Fig. 4b) caused by the strong correlations among the SOUL particles. Just as in Sec. 4.1, PGA, PQN, and PMGA all run significantly faster than SOUL due to the former three's vectorization, and the gap also widens with  $N$  (Tab. 1).

Table 1: **Bayesian neural network.** Test errors achieved using the final particle cloud  $X_K^N$ , with  $K = 500$  and  $N = 1, 10, 100$ , and corresponding computation times (averaged over 10 replicates).

	$N = 1$		$N = 10$		$N = 100$	
	Error (%)	Time (s)	Error (%)	Time (s)	Error (%)	Time (s)
PGA	$7.45 \pm 2.03$	$4.10 \pm 0.26$	$3.20 \pm 1.12$	$10.4 \pm 1.2$	$2.45 \pm 0.99$	$76.6 \pm 0.4$
PQN	$7.45 \pm 1.60$	$4.12 \pm 0.21$	$3.45 \pm 1.04$	$10.0 \pm 0.2$	$2.34 \pm 0.81$	$74.0 \pm 0.3$
PMGA	$7.24 \pm 1.75$	$3.27 \pm 0.13$	$3.75 \pm 1.38$	$9.12 \pm 0.2$	$2.45 \pm 0.81$	$72.1 \pm 0.5$
SOUL	$6.25 \pm 1.54$	$5.02 \pm 0.20$	$7.25 \pm 1.38$	$36.5 \pm 0.1$	$6.85 \pm 1.42$	$364.0 \pm 5.3$



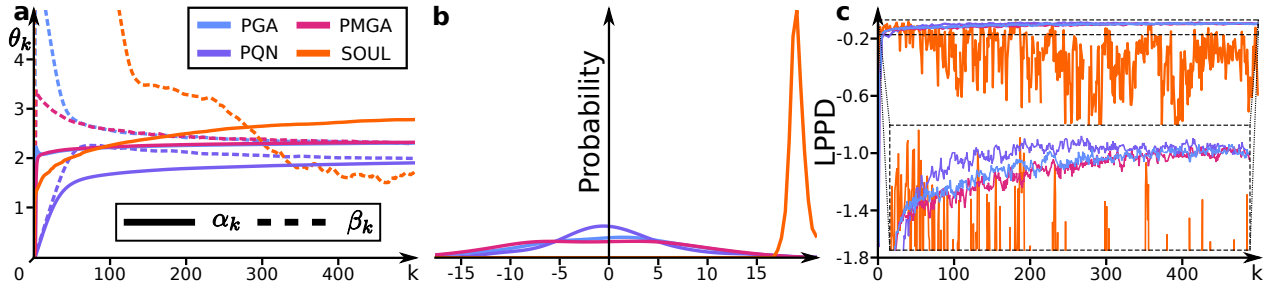


Figure 4: **Bayesian neural network.** **a** Parameter estimates as a function of  $k$  with  $N = 100$  particles and step size of  $h = 0.1$ . **b** KDE of a randomly-chosen entry of the final cloud  $X_{500}^{1:100}$ . **c** Log pointwise predictive density as a function of  $k$ . **c, inset** c zoomed-in to y-axis range  $[-0.16, -0.08]$ .

## 5 Discussion

By viewing the problem that EM tackles as a joint problem over  $\theta$  and  $q$  rather than an alternating-coordinate-wise one, we open the door to numerous new algorithms for solving the problem (be they, for instance, optimization-inspired ones, along the lines of those in Sec. 2, or purely Monte-Carlo ones of the type in App. I). This, of course, is not entirely unprecedented: even in p.6 of our starting point [48], the authors mention in passing the possibility of optimizing  $F$  ‘simultaneously’ over  $\theta$  and  $q$ , and this idea has been taken up enthusiastically in the VI literature, e.g. [36, Sec. 2]. However, outside of variational inference, we have struggled to locate papers following up on the idea.

We propose three particle-based alternatives to the EM algorithm (PGA, PQN, and PMGA in Sec. 2). Practically, we find these algorithms appealing because they are simple to implement and tune, apply to broad classes of models (i.e. those on Euclidean spaces with differentiable densities), and, above all, are scalable. In particular, their complexity is linear with the dimension of the latent variables and, at least for PGA, that of the parameters too. For most models in the literature (e.g. those for which the data is conditionally independent given the latent variables and parameters), it is also linear in the dimension of the data. For big-data scenarios where the latter linear complexity proves a limiting factor, we advise simply replacing the gradients in (9,12,13,15) with stochastic estimates thereof (as in [58, 68, 49]) — this type of approach will likely benefit from encouraging exploration by using different subsamplings of the data to update different particles. Furthermore, much like in [20], we circumvent the degeneracy with latent-variable dimension that plagues common MCMC methods (e.g. see [5, 65, 39, 40] and references therein) by avoiding accept-reject steps and employing ULA kernels (known to have favourable properties [18, 25, 26]). Lastly, computations within our algorithms are easily vectorized across particles: a significant boon in practice (Sect. 4, see also the discussion of ‘parallel SGLD’ in [42, p. 7] for similar observations).

Theoretically, we find PGA, PQN, and PMGA attractive because they re-use the previously computed posterior approximation at each update step; and ‘warm-starts’ along these lines are known to be beneficial for methods reliant on the ULA kernel [18, 25, 26]. This stands in contrast with previous Monte Carlo EM alternatives [67, 38, 32, 21, 71, 37, 11, 54, 20] which, at best, initialize the chain for the parameter current update at the final state of the preceding update’s chain. This resulted in our methods achieving better performance for models with complex multimodal posteriors (Sec. 4.2). Of course, it proved a disadvantage for models with simple peaked unimodal posteriors where piecemeal evolving an entire particle cloud leads to long transients for poor initializations (Sec. 4.1). However, this issue was easily mitigated by warm-starting our algorithms using a preliminary  $N = 1$  run.

We see several interesting lines of future work including (a) the theoretical analysis of the algorithms proposed in this paper, (b) the study of variants thereof, and (c) the investigation of other particle-based methods obtained by viewing the EM problem ‘jointly over  $\theta$  and  $q$ ’ rather than in a coordinate-wise manner. For (a), we believe that [18, 25, 26, 20] might be good jumping-off points. Aside from the big-data tweaks mentioned above, for (b) we have in mind adapting the step sizes and particle numbers as we go along: it seems natural to use cruder posterior approximations and larger step sizes early on in  $F$ ’s optimization, cf. [67, 32, 21, 71, 37, 11, 20, 58] for similar ideas. In particular, by decreasing the step size  $h$  and increasing the

particle number  $N$  with the step number  $k$ , it is likely possible to eliminate the asymptotic bias from our algorithms (Sect. 3). To adapt the step size, it be beneficial to use a more modern scheme along the lines of Adagrad and its variants, e.g. see [59]. For (c), this might amount to switching the geometry on  $\Theta \times \mathcal{P}(\mathcal{X})$  w.r.t. which we define gradients and following a discretization procedure analogous to that in Sec. 2.1. For instance, using a Stein geometry leads to an generalization of [42] which makes more extensive use of the particle cloud at the price of a higher computational cost. Alternatively, one could search for analogues of other well-known optimization algorithms applied to  $F$  aside from gradient ascent (e.g. one for Nesterov acceleration along the lines of [44, 16, 62, 66]) or a Metropolis-Hastings method of the type in App. I.

**Limitations.** Our algorithms, like EM and most alternatives thereof (but not all, e.g. [23, 34]), only return stationary points of the marginal likelihood and not necessarily global optima. Moreover, at least as presented here, our algorithms are limited to Euclidean parameter and latent spaces and models with differentiable densities. This said, they apply almost unchanged were the spaces to be Riemannian manifolds (e.g. see [7]) — extensions to other spaces are less obvious and require finding a sensible analogue of the Euclidean gradient that can be evaluated pointwise. Furthermore, some of the common non-differentiabilities can be dealt with by incorporating proximal operators into our algorithms along the lines of [51, 53, 28, 27, 4, 30, 19, 61, 60].

**Acknowledgements** We thank Valentin De Bortoli, Arnaud Doucet, and Jordan Ang for insightful discussions. JK and AMJ acknowledge support from the Engineering and Physical Sciences Research Council (EPSRC; grant # EP/T004134/1) and the Lloyd’s Register Foundation Programme on Data-Centric Engineering at the Alan Turing Institute. AMJ acknowledge further support from the EPSRC (grant # EP/R034710/1).

## References

- [1] L. Ambrosio, N. Gigli, and G. Savaré. *Gradient flows: in metric spaces and in the space of probability measures*. Birkhäuser Basel, 2005. URL <https://doi.org/10.1007/b137080>.
- [2] C. Andrieu, N. de Freitas, A. Doucet, and M. I. Jordan. An introduction to MCMC for machine learning. *Machine Learning*, 50:5–43, 2003. URL <https://doi.org/10.1023/A:1020281327116>.
- [3] A. Arnold, P. Markowich, G. Toscani, and A. Unterreiter. On convex Sobolev inequalities and the rate of convergence to equilibrium for Fokker-Planck type equations. *Communications in Partial Differential Equations*, 26(1-2):43–100, 2001. URL <https://doi.org/10.1081/PDE-100002246>.
- [4] E. Bernton. Langevin Monte Carlo and JKO splitting. In *Proceedings of the 31st Conference On Learning Theory*, volume 75 of *PMLR*, pages 1777–1798, 2018. URL <https://proceedings.mlr.press/v75/bernton18a.html>.
- [5] A. Beskos, N. Pillai, G. Roberts, J.-M. Sanz-Serna, and A. Stuart. Optimal tuning of the hybrid Monte Carlo algorithm. *Bernoulli*, 19(5A):1501–1534, 2013. URL <https://doi.org/10.3150/12-BEJ414>.
- [6] C. M. Bishop. *Pattern Recognition and Machine Learning*. Springer New York, 2006.
- [7] N. Boumal. An introduction to optimization on smooth manifolds. To appear with Cambridge University Press, 2022. URL <http://www.nicolasboumal.net/book>.
- [8] S. P. Boyd and L. Vandenberghe. *Convex Optimization*. Cambridge University Press, 2004. URL <https://doi.org/10.1017/CB09780511804441>.
- [9] J. Bradbury, R. Frostig, P. Hawkins, M. J. Johnson, C. Leary, D. Maclaurin, G. Necula, A. Paszke, J. VanderPlas, S. Wanderman-Milne, and Q. Zhang. JAX: composable transformations of Python+NumPy programs, 2018. URL <http://github.com/google/jax>.
- [10] H. J. Brascamp and E. H. Lieb. On extensions of the Brunn-Minkowski and Prékopa-Leindler theorems, including inequalities for log concave functions, and with an application to the diffusion equation. *Journal of Functional Analysis*, 22(4):366–389, 1976. URL [https://doi.org/10.1016/0022-1236\(76\)90004-5](https://doi.org/10.1016/0022-1236(76)90004-5).

- [11] L. Cai. High-dimensional exploratory item factor analysis by a Metropolis-Hastings Robbins-Monro algorithm. *Psychometrika*, 75(1):33–57, 2010. URL <https://doi.org/10.1007/s11336-009-9136-x>.
- [12] J. A. Carrillo, R. S. Gvalani, and J. Wu. An invariance principle for gradient flows in the space of probability measures. *arXiv preprint arXiv:2010.00424*, 2020. URL <https://arxiv.org/abs/2010.00424>.
- [13] L.-P. Chaintron and A. Diez. Propagation of chaos: a review of models, methods and applications. I. Models and methods. *arXiv preprint arXiv:2203.00446*, 2022. URL <https://arxiv.org/abs/2203.00446>.
- [14] C. Chen, R. Zhang, W. Wang, B. Li, and L. Chen. In *Conference on Uncertainty in Artificial Intelligence (UAI)*, 2018. URL <http://auai.org/uai2018/proceedings/papers/263.pdf>.
- [15] X. Cheng and P. Bartlett. Convergence of Langevin MCMC in KL-divergence. In *Proceedings of Algorithmic Learning Theory*, volume 83, pages 186–211, 2018. URL <https://proceedings.mlr.press/v83/cheng18a.html>.
- [16] X. Cheng, N. S. Chatterji, P. L. Bartlett, and M. I. Jordan. Underdamped Langevin MCMC: A non-asymptotic analysis. In *Proceedings of the 31st Conference On Learning Theory*, volume 75 of *PMLR*, pages 300–323, 2018. URL <https://proceedings.mlr.press/v75/cheng18a.html>.
- [17] I. Csiszár and G. Tusnády. Information geometry and alternating minimization procedures. *Statistics and decisions*, Supp. 1:205–237, 1984.
- [18] A. S. Dalalyan. Theoretical guarantees for approximate sampling from smooth and log-concave densities. *Journal of the Royal Statistical Society: Series B (Statistical Methodology)*, 79(3):651–676, 2017. URL <https://doi.org/10.1111/rssb.12183>.
- [19] V. De Bortoli, A. Durmus, M. Pereyra, and A. Fernandez Vidal. Maximum Likelihood Estimation of Regularization Parameters in High-Dimensional Inverse Problems: An Empirical Bayesian Approach. Part II: Theoretical Analysis. *SIAM Journal on Imaging Sciences*, 13(4):1990–2028, 2020. URL <https://doi.org/10.1137/20M1339842>.
- [20] V. De Bortoli, A. Durmus, M. Pereyra, and A. Fernandez Vidal. Efficient stochastic optimisation by unadjusted Langevin Monte Carlo. *Statistics and Computing*, 31, 2021. URL <https://doi.org/10.1007/s11222-020-09986-y>.
- [21] B. Delyon, M. Lavielle, and É. Moulines. Convergence of a stochastic approximation version of the EM algorithm. *The Annals of Statistics*, 27(1):94–128, 1999. URL <http://www.jstor.org/stable/120120>.
- [22] A. P. Dempster, N. M. Laird, and D. B. Rubin. Maximum likelihood from incomplete data via the EM algorithm. *Journal of the Royal Statistical Society: Series B (Methodological)*, 39(1):1–22, 1977. URL <https://doi.org/10.1111/j.2517-6161.1977.tb01600.x>.
- [23] A. Doucet, S. J. Godsill, and C. P. Robert. Marginal maximum a posteriori estimation using Markov chain Monte Carlo. *Statistics and Computing*, 12:77–84, 2002. URL <https://doi.org/10.1023/A:1013172322619>.
- [24] A. Duncan, N. Nuesken, and L. Szpruch. On the geometry of Stein variational gradient descent. *arXiv preprint arXiv:1912.00894*, 2019. URL <https://arxiv.org/abs/1912.00894>.
- [25] A. Durmus and É. Moulines. Nonasymptotic convergence analysis for the unadjusted Langevin algorithm. *The Annals of Applied Probability*, 27(3):1551–1587, 2017. URL <https://doi.org/10.1214/16-AAP1238>.
- [26] A. Durmus and É. Moulines. High-dimensional Bayesian inference via the unadjusted Langevin algorithm. *Bernoulli*, 25(4A):2854–2882, 2019. URL <https://doi.org/10.3150/18-BEJ1073>.
- [27] A. Durmus, É. Moulines, and M. Pereyra. Efficient Bayesian Computation by Proximal Markov Chain Monte Carlo: When Langevin Meets Moreau. *SIAM Journal on Imaging Sciences*, 11(1):473–506, 2018. URL <https://doi.org/10.1137/16M1108340>.

- [28] A. Durmus, S. Majewski, and B. Miasojedow. Analysis of Langevin Monte Carlo via Convex Optimization. *Journal of Machine Learning Research*, 20(73):1–46, 2019. URL <http://jmlr.org/papers/v20/18-173.html>.
- [29] D. L. Ermak. A computer simulation of charged particles in solution. I. Technique and equilibrium properties. *The Journal of Chemical Physics*, 62(10):4189–4196, 1975. URL <https://doi.org/10.1063/1.430300>.
- [30] A. Fernandez Vidal, V. De Bortoli, M. Pereyra, and A. Durmus. Maximum Likelihood Estimation of Regularization Parameters in High-Dimensional Inverse Problems: An Empirical Bayesian Approach Part I: Methodology and Experiments. *SIAM Journal on Imaging Sciences*, 13(4):1945–1989, 2020. URL <https://doi.org/10.1137/20M1339829>.
- [31] A. Garbuno-Inigo, F. Hoffmann, W. Li, and A. M. Stuart. Interacting Langevin diffusions: Gradient structure and ensemble Kalman sampler. *SIAM Journal on Applied Dynamical Systems*, 19(1):412–441, 2020. URL <https://doi.org/10.1137/19M1251655>.
- [32] Ming Gao Gu and Fan Hui Kong. A stochastic approximation algorithm with Markov chain Monte-Carlo method for incomplete data estimation problems. *Proceedings of the National Academy of Sciences*, 95(13):7270–7274, 1998. URL <https://doi.org/10.1073/pnas.95.13.7270>.
- [33] M. Hauray and S. Mischler. On Kac’s chaos and related problems. *Journal of Functional Analysis*, 266(10):6055–6157, 2014. URL <https://doi.org/10.1016/j.jfa.2014.02.030>.
- [34] A. M. Johansen, A. Doucet, and M. Davy. Particle methods for maximum likelihood parameter estimation in latent variable models. *Statistics and Computing*, 18(1):47–57, 2008. URL <https://doi.org/10.1007/s11222-007-9037-8>.
- [35] R. Jordan, D. Kinderlehrer, and F. Otto. The variational formulation of the Fokker–Planck equation. *SIAM Journal on Mathematical Analysis*, 29(1):1–17, 1998. URL <https://doi.org/10.1137/S0036141096303359>.
- [36] D. P. Kingma and M. Welling. An introduction to variational autoencoders. *Foundations and Trends® in Machine Learning*, 12(4):307–392, 2019. URL <https://doi.org/10.1561/22000000056>.
- [37] E. Kuhn and M. Lavielle. Coupling a stochastic approximation version of EM with an MCMC procedure. *ESAIM: Probability and Statistics*, 8:115–131, 2004. URL <https://doi.org/10.1051/ps:2004007>.
- [38] Anthony Y. C. Kuk and Yuk W. Cheng. The Monte Carlo Newton–Raphson algorithm. *Journal of Statistical Computation and Simulation*, 59(3):233–250, 1997. URL <https://doi.org/10.1080/00949657708811858>.
- [39] J. Kuntz, M. Ottobre, and A. M. Stuart. Non-stationary phase of the MALA algorithm. *Stochastics and Partial Differential Equations: Analysis and Computations*, 6:446–499, 2019. URL <https://doi.org/10.1007/s40072-018-0113-1>.
- [40] J. Kuntz, M. Ottobre, and A. M. Stuart. Diffusion limit for the random walk Metropolis algorithm out of stationarity. *Annales de l’Institut Henri Poincaré, Probabilités et Statistiques*, 55(3):1599–1648, 2019. URL <https://doi.org/10.1214/18-AIHP929>.
- [41] Y. Lecun, L. Bottou, Y. Bengio, and P. Haffner. Gradient-based learning applied to document recognition. *Proceedings of the IEEE*, 86(11):2278–2324, 1998. URL <https://doi.org/10.1109/5.726791>.
- [42] Qiang Liu and Dilin Wang. Stein variational gradient descent: A general purpose Bayesian inference algorithm. In *Advances in Neural Information Processing Systems*, volume 29, 2016. URL <https://proceedings.neurips.cc/paper/2016/file/b3ba8f1bee1238a2f37603d90b58898d-Paper.pdf>.
- [43] Y. Lu, J. Lu, and J. Nolen. Accelerating Langevin sampling with birth-death. *arXiv preprint arXiv:1905.09863*, 2019. URL <https://arxiv.org/abs/1905.09863>.

- [44] Y.-A. Ma, N. S. Chatterji, X. Cheng, N. Flammarion, P. Bartlett, and M. I. Jordan. Is there an analog of Nesterov acceleration for MCMC? *arXiv preprint arXiv:1902.00996*, 2019. URL <https://arxiv.org/abs/1902.00996>.
- [45] P. A. Markowich and C. Villani. On the trend to equilibrium for the Fokker-Planck equation: an interplay between physics and functional analysis. *Matemática Contemporânea (SBM)*, 19:1–29, 2000. URL <http://mc.sbm.org.br/wp-content/uploads/sites/9/sites/9/2021/12/19-1.pdf>.
- [46] J. Martens. New insights and perspectives on the natural gradient method. *Journal of Machine Learning Research*, 21(146):1–76, 2020. URL <http://jmlr.org/papers/v21/17-678.html>.
- [47] T. McLachlan, G. J. Krishnan. *The EM Algorithm and Extensions*. John Wiley & Sons, 2nd edition, 2007. URL <https://doi.org/10.1002/9780470191613>.
- [48] R. M. Neal and G. E. Hinton. A view of the EM algorithm that justifies incremental, sparse, and other variants. In *Learning in Graphical Models*, pages 355–368. Springer Netherlands, 1998. URL [https://doi.org/10.1007/978-94-011-5014-9\\_12](https://doi.org/10.1007/978-94-011-5014-9_12).
- [49] C. Nemeth and P. Fearnhead. Stochastic gradient markov chain monte carlo. *Journal of the American Statistical Association*, 116(533):433–450, 2021. URL <https://doi.org/10.1080/01621459.2020.1847120>.
- [50] Felix Otto. The geometry of dissipative evolution equations: the porous medium equation. *Communications in Partial Differential Equations*, 26(1-2):101–174, 2001. URL <https://doi.org/10.1081/PDE-100002243>.
- [51] N. Parikh and S. Boyd. Proximal algorithms. *Foundations and Trends® in Optimization*, 1(3):127–239, 2014. URL <https://doi.org/10.1561/24000000003>.
- [52] G. Parisi. Correlation functions and computer simulations. *Nuclear Physics B*, 180(3):378–384, 1981. URL [https://doi.org/10.1016/0550-3213\(81\)90056-0](https://doi.org/10.1016/0550-3213(81)90056-0).
- [53] M. Pereyra. Proximal Markov chain Monte Carlo algorithms. *Statistics and Computing*, 26(4):745–760, 2016. URL <https://doi.org/10.1007/s11222-015-9567-4>.
- [54] Y. Qiu and X. Wang. Stochastic approximate gradient descent via the Langevin algorithm. *Proceedings of the AAAI Conference on Artificial Intelligence*, 34(4):5428–5435, 2020. URL <https://doi.org/10.1609/aaai.v34i04.5992>.
- [55] Gareth O. R. and Richard L. T. Exponential convergence of Langevin distributions and their discrete approximations. *Bernoulli*, 2(4):341–363, 1996. URL <https://doi.org/10.2307/3318418>.
- [56] S. Reich and S. Weissmann. Fokker–Planck particle systems for Bayesian inference: Computational approaches. *SIAM/ASA Journal on Uncertainty Quantification*, 9(2):446–482, 2021. URL <https://doi.org/10.1137/19M1303162>.
- [57] H. Robbins. An empirical Bayes approach to statistics. In *Proceedings of the Third Berkeley Symposium on Mathematical Statistics and Probability*, volume 3.1, pages 157–164, 1956.
- [58] H. Robbins and S. Monro. A stochastic approximation method. *The Annals of Mathematical Statistics*, 22(3):400–407, 1951. URL <http://www.jstor.org/stable/2236626>.
- [59] S. Ruder. An overview of gradient descent optimization algorithms. *arXiv preprint arXiv:1609.04747*, 2016. URL <https://arxiv.org/abs/1609.04747>.
- [60] A. Salim and P. Richtarik. Primal Dual Interpretation of the Proximal Stochastic Gradient Langevin Algorithm. In *Advances in Neural Information Processing Systems*, volume 33, pages 3786–3796, 2020. URL <https://proceedings.neurips.cc/paper/2020/file/2779fda014fbadb761f67dd708c1325e-Paper.pdf>.



- [61] A. Salim, A. Korba, and Giulia Luise. The Wasserstein Proximal Gradient Algorithm. In *Advances in Neural Information Processing Systems*, volume 33, pages 12356–12366, 2020. URL <https://proceedings.neurips.cc/paper/2020/file/91cff01af640a24e7f9f7a5ab407889f-Paper.pdf>.
- [62] A. Taghvaei and P. Mehta. Accelerated flow for probability distributions. In *Proceedings of the 36th International Conference on Machine Learning*, volume 97 of *PMLR*, pages 6076–6085, 2019. URL <https://proceedings.mlr.press/v97/taghvaei19a.html>.
- [63] A. Vehtari, A. Gelman, and Gabry. Practical Bayesian model evaluation using leave-one-out cross-validation and WAIC. *Statistics and Computing*, 27(5):1413–1432, 2017. URL <https://doi.org/10.1007/s11222-016-9696-4>.
- [64] C. Villani. *Optimal Transport: Old and New*. Springer, Berlin, Heidelberg, 2009. URL <https://doi.org/10.1007/978-3-540-71050-9>.
- [65] J. Vogrinc, S. Livingstone, and G. Zanella. Optimal design of the Barker proposal and other locally-balanced Metropolis-Hastings algorithms. *arXiv preprint arXiv:2201.01123*, 2022. URL <https://arxiv.org/abs/2201.01123>.
- [66] Y. Wang and W. Li. Accelerated information gradient flow. *Journal of Scientific Computing*, 90(11), 2022. URL <https://doi.org/10.1007/s10915-021-01709-3>.
- [67] G. C. G. Wei and M. A. Tanner. A Monte Carlo implementation of the EM algorithm and the poor man’s data augmentation algorithms. *Journal of the American Statistical Association*, 85(411):699–704, 1990. URL <https://doi.org/10.1080/01621459.1990.10474930>.
- [68] M. Welling and Y. W. Teh. Bayesian learning via stochastic gradient Langevin dynamics. In *Proceedings of the 28th International Conference on Machine Learning (ICML)*, pages 681–688, 2011. URL [https://icml.cc/Conferences/2011/papers/398\\_icmlpaper.pdf](https://icml.cc/Conferences/2011/papers/398_icmlpaper.pdf).
- [69] W. H. Wolberg and O. L. Mangasarian. Multisurface method of pattern separation for medical diagnosis applied to breast cytology. *Proceedings of the National Academy of Sciences*, 87(23):9193–9196, 1990. doi: 10.1073/pnas.87.23.9193. URL <https://doi.org/10.1073/pnas.87.23.9193>.
- [70] Y. Yao, A. Vehtari, and A. Gelman. Stacking for non-mixing Bayesian computations: The curse and blessing of multimodal posteriors. *arXiv preprint arXiv:2006.12335*, 2020. URL <https://arxiv.org/abs/2006.12335>.
- [71] L. Younes. On the convergence of Markovian stochastic algorithms with rapidly decreasing ergodicity rates. *Stochastics and Stochastic Reports*, 65(3–4):177–228, 1999. URL <https://doi.org/10.1080/17442509908834179>.
- [72] C. Zhang, Z. Li, H. Qian, and X. Du. Dpvi: A dynamic-weight particle-based variational inference framework. *arXiv preprint arXiv:2112.00945*, 2021. URL <https://arxiv.org/abs/2112.00945>.

## A An informal crash course in calculus on $\Theta \times \mathcal{P}(\mathcal{X})$

This appendix assumes that the reader is familiar with rudimentary Riemannian geometry not exceeding the level of [7, Chap. 3].

Otto et al.’s brilliant observation [35, 50] was that, even though  $\mathcal{P}(\mathcal{X})$  is not technically a Riemannian manifold, we can often treat it as one and apply the rules we have for calculus on Riemannian manifolds almost unchanged. While rigorously establishing these facts is an involved matter [1, 64], the basic ideas are very accessible. Here we review these ideas, but in the slightly generalized setting of  $\mathcal{M} := \Theta \times \mathcal{P}(\mathcal{X})$ . To treat  $\mathcal{M}$  as a Riemannian manifold we require three things:

- for each  $(\theta, q)$  in  $\mathcal{M}$ , a tangent space  $\mathcal{T}_{(\theta, q)}\mathcal{M}$ : a linear space describing the directions we can move if we are at  $(\theta, q)$ ;



- for each  $(\theta, q)$  in  $\mathcal{M}$ , a cotangent space  $\mathcal{T}_{(\theta, q)}^* \mathcal{M}$  dual to  $\mathcal{T}_{(\theta, q)} \mathcal{M}$  with a duality pairing

$$\langle \cdot, \cdot \rangle_{(\theta, q)} : \mathcal{T}_{(\theta, q)} \mathcal{M} \times \mathcal{T}_{(\theta, q)}^* \mathcal{M} \rightarrow \mathbb{R};$$

- and a Riemannian metric  $g = (g_{(\theta, q)})_{(\theta, q) \in \mathcal{M}}$ , where  $g_{(\theta, q)}$  denotes an inner product on  $\mathcal{T}_{(\theta, q)} \mathcal{M}$  for each  $(\theta, q)$  in  $\mathcal{M}$ .

Once we have chosen the above, defining a sensible notion for the gradient of a functional on  $\mathcal{M}$  will be a simple matter.

**An abuse of notation.** The tangent spaces  $(\mathcal{T}_{(\theta, q)} \mathcal{M})_{(\theta, q) \in \mathcal{M}}$  that we use will be copies of a single space  $\mathcal{T}\mathcal{M}$  (and, in particular, independent of  $(\theta, q)$ ). Hence, we drop the  $(\theta, q)$  subscripts to simplify the notation. The cotangent spaces and duality pairings will also be independent of  $(\theta, q)$  and we similarly simplify our notation.

## A.1 Tangent and cotangent spaces

$\mathcal{M}$  is defined as the product of  $\Theta$  and  $\mathcal{P}(\mathcal{X})$ , so we find sensible tangent spaces,  $\mathcal{T}\Theta$  and  $\mathcal{T}\mathcal{P}(\mathcal{X})$ , for these two and define that for  $\mathcal{M}$  to be the product:

$$\mathcal{T}\mathcal{M} = \mathcal{T}\Theta \times \mathcal{T}\mathcal{P}(\mathcal{X}).$$

The cotangent spaces then obey an analogous relationship,

$$\mathcal{T}^* \mathcal{M} = \mathcal{T}^* \Theta \times \mathcal{T}^* \mathcal{P}(\mathcal{X}),$$

and we can express the duality pairing for  $(\mathcal{T}\mathcal{M}, \mathcal{T}^* \mathcal{M})$  in terms of those for  $(\mathcal{T}\Theta, \mathcal{T}^* \Theta)$  and  $(\mathcal{T}\mathcal{P}(\mathcal{X}), \mathcal{T}^* \mathcal{P}(\mathcal{X}))$ :

$$\langle (\tau, m), (v, f) \rangle = \langle \tau, v \rangle + \langle m, f \rangle \quad \forall (\tau, m) \in \mathcal{T}\mathcal{M}, (v, f) \in \mathcal{T}^* \mathcal{M}.$$

**Tangent and cotangent spaces for  $\Theta$ .** Throughout the paper we focus on Euclidean parameter spaces ( $\Theta = \mathbb{R}^{D_\theta}$ ), in which case the tangent spaces are just copies of the parameter space:  $\mathcal{T}\Theta = \mathbb{R}^{D_\theta}$ . The cotangent spaces are also copies of  $\mathbb{R}^{D_\theta}$  and the duality pairing is the Euclidean inner product:

$$\langle \tau, v \rangle := \sum_{i=1}^{D_\theta} \tau_i v_i \quad \forall \tau \in \mathcal{T}\Theta, v \in \mathcal{T}^* \Theta.$$

The above said, modulo the re-insertion of  $\theta$  subscripts, the ensuing discussion would apply unchanged were  $\Theta$  to be any sufficiently-differentiable finite-dimensional Riemannian manifold.

**Tangent and cotangent spaces for  $\mathcal{P}(\mathcal{X})$ .** To keep the exposition simple, we restrict  $\mathcal{P}(\mathcal{X})$  to the set of probability measures with strictly positive densities w.r.t. to the Lebesgue measure  $dx$  and identify a measure with its density. (Circumventing this restriction and giving a full rigorous treatment of our results requires employing the techniques of [1], which we abstain from doing here.) With this restriction, the tangent spaces are simple and do not depend on  $q$ :

$$\mathcal{T}\mathcal{P}(\mathcal{X}) := \left\{ \text{functions } m : \mathcal{X} \rightarrow \mathbb{R} \text{ satisfying } \int m(x) dx = 0 \right\}.$$

The cotangent spaces can be identified with the space of equivalence classes of measurable functions that differ by an additive constant,

$$\mathcal{T}^* \mathcal{P}(\mathcal{X}) := \{f : \mathbb{R}^n \rightarrow \mathbb{R}\} / \mathbb{R};$$

and the duality pairing is given by

$$\langle m, f \rangle := \int f(x) m(x) dx \quad \forall m \in \mathcal{T}\mathcal{P}(\mathcal{X}), f \in \mathcal{T}^* \mathcal{P}(\mathcal{X}).$$

Note that, in the above and throughout, we commit the usual notational abuse using  $f$  to denote both a function and the equivalence class to which it belongs. We also tacitly assume that the measurability and integrability conditions required for our integrals to make sense are satisfied.

## A.2 Riemannian metrics

We define each metric  $g = (g_{(\theta,q)})_{(\theta,q) \in \mathcal{M}}$  in terms of a *tensor*  $G = (G_{(\theta,q)})_{(\theta,q) \in \mathcal{M}}$  and the duality pairing:

$$g_{(\theta,q)}((\tau, m), (\tau', m')) := \langle (\tau, m), G_{(\theta,q)}(\tau', m') \rangle \quad \forall (\theta, q) \in \mathcal{M}.$$

By a tensor  $G$  we mean a collection indexed by  $(\theta, q)$  in  $\mathcal{M}$  of invertible, self-adjoint, positive-definite, linear maps from  $\mathcal{TM}$  to  $\mathcal{T}^*\mathcal{M}$ . Most of the tensors  $G_{(\theta,q)}$  we will consider are ‘block-diagonal’:

$$\langle (\tau, m), G_{(\theta,q)}(\tau', m') \rangle = \langle \tau, G_{(\theta,q)}\tau' \rangle + \langle m, G_{(\theta,q)}m' \rangle =: \mathbf{g}_{(\theta,q)}(\tau, \tau') + \mathbf{g}_{(\theta,q)}(m, m'),$$

where  $G_{(\theta,q)}$  and  $G_{(\theta,q)}$  respectively denote tensors on  $\Theta$  and  $\mathcal{P}(\mathcal{X})$ . In this case, we write  $\text{diag}(G_{(\theta,q)}, G_{(\theta,q)})$  for  $G_{(\theta,q)}$ . If any of the above do not depend on  $\theta$ , we omit it from the subscript, and similarly for  $q$ .

Although there are many options that one could consider for the  $G_{(\theta,q)}$  block (e.g. see [24, 31, 43]), we focus on two, the first for practical reasons and the second for theoretical ones:

**Wasserstein-2.** The tensor  $G_q^W$  is defined by its inverse

$$(G_q^W)^{-1}f := -\nabla_x \cdot (q \nabla_x f). \quad (18)$$

Using integration-by-parts, we find that

$$\mathbf{g}_q^W(m, m') = \int \langle \nabla_x f(x), \nabla_x f'(x) \rangle q(x) dx \quad \forall q \in \mathcal{P}(\mathcal{X}),$$

where  $f, f'$  are the unique (up to an additive constant) solutions to  $m = (G_q^W)^{-1}f$  and  $m' = (G_q^W)^{-1}f'$  and  $\langle \cdot, \cdot \rangle$  denotes the Euclidean inner product on  $\mathbb{R}^{D_x}$ . The tensor’s name stems from the fact that the distance metric induced by  $\mathbf{g}_q^W$  on  $\mathcal{P}(\mathcal{X})$  coincides with the Wasserstein-2 distance from optimal transport, e.g. [1, p. 168].

**Fisher-Rao.** The tensor is  $G_q^{FR}m := m/q$  and has inverse

$$((G_q^{FR})^{-1}f)(x) = q(x) \left[ f(x) - \int f(x)q(x)dx \right]. \quad (19)$$

Hence,

$$\mathbf{g}_q^{FR}(m, m') := \int \frac{m(x)}{q(x)} \frac{m'(x)}{q(x)} q(x) dx \quad \forall q \in \mathcal{P}(\mathcal{X}).$$

Its name stems from the fact that the usual Fisher-Rao metric on a parameter space  $\Lambda \subseteq \mathbb{R}^{D_\lambda}$  indexing a parametric family  $\mathcal{Q} := (q_\lambda)_{\lambda \in \Lambda}$  is obtained by pulling  $\mathbf{g}_q^{FR}$  back through  $\lambda \mapsto q_\lambda$ :

$$\begin{aligned} \mathbf{g}_\lambda^{\text{pullback}}(\beta, \beta') &= \mathbf{g}_{q_\lambda}^{FR}(\langle \beta, \nabla_\lambda q_\lambda \rangle, \langle \beta', \nabla_\lambda q_\lambda \rangle) = \int \frac{\langle \beta, \nabla_\lambda q_\lambda(x) \rangle}{q_\lambda(x)} \frac{\langle \beta', \nabla_\lambda q_\lambda(x) \rangle}{q_\lambda(x)} q_\lambda(x) dx \\ &= \int \langle \beta, \nabla_\lambda \log(q_\lambda(x)) \rangle \langle \beta', \nabla_\lambda \log(q_\lambda(x)) \rangle q_\lambda(x) dx = \langle \beta, \mathcal{I}^\lambda \beta' \rangle, \end{aligned}$$

where  $\mathcal{I}^\lambda$  denotes the Fisher information matrix, i.e.

$$\mathcal{I}^\lambda := \left( \int \frac{\partial \log(q_\lambda)}{\partial \lambda_i}(x) \frac{\partial \log(q_\lambda)}{\partial \lambda_j}(x) q_\lambda(x) dx \right)_{ij=1}^{D_\lambda}.$$

## A.3 Gradients

Given a Riemannian metric  $g$  on  $\mathcal{M}$ , the gradient of a functional  $E$  on  $\mathcal{M}$  is defined as the unique vector field  $\nabla^g E : \mathcal{M} \rightarrow \mathcal{TM}$  satisfying

$$g_{(\theta,q)}(\nabla^g E(\theta, q), (\tau, m)) = \lim_{t \rightarrow 0} \frac{E(\theta + t\tau, q + tm) - E(\theta, q)}{t} \quad \forall (\tau, m) \in \mathcal{TM}, \quad (\theta, q) \in \mathcal{M}. \quad (20)$$

The following identity often simplifies gradient calculations:

$$\nabla^g E(\theta, q) = G_{\theta, q}^{-1} \delta E(\theta, q) \quad \forall (\theta, q) \in \mathcal{M}, \quad (21)$$

where  $\delta E : \mathcal{M} \rightarrow \mathcal{T}^* \mathcal{M}$  denotes  $E$ 's *first variation*<sup>3</sup>: the unique cotangent vector field satisfying

$$\langle (\tau, m), \delta E(\theta, q) \rangle = \lim_{t \rightarrow 0} \frac{E(\theta + t\tau, q + tm) - E(\theta, q)}{t} \quad \forall (\tau, m) \in \mathcal{TM}, \quad (\theta, q) \in \mathcal{M}. \quad (22)$$

In turn,  $\delta E$ 's computation can be simplified using  $\delta E = (\delta_\theta E, \delta_q E)$ , where  $\delta_\theta$  and  $\delta_q$  denote the first variations on  $\Theta$  and  $\mathcal{P}(\mathcal{X})$  (defined analogously to (22) but for the maps  $\theta \mapsto E(\theta, q)$  and  $q \mapsto E(\theta, q)$ , respectively).

**Lemma 1.** *In the case of the free energy,  $F$  in (1),  $\delta F(\theta, q) = (\delta_\theta F(\theta, q), \delta_q F(\theta, q))$  where*

$$\delta_\theta F(\theta, q) = \int \nabla_\theta \ell(\theta, x) q(x) dx, \quad \delta_q F(\theta, q) = \log \left( \frac{p_\theta(\cdot, y)}{q} \right), \quad \forall (\theta, q) \in \mathcal{M}.$$

*Proof.* We need to show that, for any given  $(\theta, q)$  in  $\mathcal{M}$ ,

$$F(\theta + t\tau, q) = F(\theta, q) + t \left\langle \tau, \int \nabla_\theta \ell(\theta, x) q(x) dx \right\rangle + o(t) \quad \forall \tau \in \mathcal{T}\Theta, \quad (23)$$

$$F(\theta, q + tm) = F(\theta, q) + t \left\langle m, \log \left( \frac{p_\theta(\cdot, y)}{q} \right) \right\rangle + o(t) \quad \forall m \in \mathcal{TP}(\mathcal{X}). \quad (24)$$

We begin with (23):  $\ell(\theta + t\tau, x) = \ell(\theta, x) + t \langle \tau, \nabla_\theta \ell(\theta, x) \rangle + o(t)$  and, so<sup>4</sup>,

$$\begin{aligned} F(\theta + t\tau, q) &= F(\theta, q) - \int \ell(\theta, x) q(x) dx + \int \ell(\theta + t\tau, x) q(x) dx \\ &= F(\theta, q) + \int [t \langle \tau, \nabla_\theta \ell(\theta, x) \rangle + o(t)] q(x) dx \\ &= F(\theta, q) + t \left\langle \tau, \int \nabla_\theta \ell(\theta, x) q(x) dx \right\rangle + o(t). \end{aligned}$$

For (24) instead note that  $\log(z + t)(z + t) = \log(z)z + [\log(z) + 1]t + o(t)$ , whence

$$\begin{aligned} F(\theta, q + tm) &= \int \ell(\theta, x)(q(x) + tm(x)) dx - \int \log(q(x) + tm(x))(q(x) + tm(x)) dx \\ &= \int \ell(\theta, x) q(x) dx + t \int \log(p_\theta(x, y)) m(x) dx \\ &\quad - \int [\log(q(x)) q(x) + [\log(q(x)) + 1] tm(x) + o(t)] dx \\ &= F(\theta, q) + t \int [\log(p_\theta(x, y)) - \log(q(x))] m(x) dx - t \int m(x) dx + o(t); \end{aligned}$$

and (24) follows because  $\int m(x) dx = 0$  given that  $m$  belongs to  $\mathcal{TP}(\mathcal{X})$  (cf. App. A.1).  $\square$

For metrics  $g$  with a block-diagonal tensor  $\text{diag}(G_{(\theta, q)}, G_{(\theta, q)})$ , we have one final simplification:

$$\nabla^g E(\theta, q) = (G_{\theta, q}^{-1} \delta_\theta E(\theta, q), G_{\theta, q}^{-1} \delta_q E(\theta, q)) \quad \forall (\theta, q) \in \mathcal{M}. \quad (25)$$

<sup>3</sup>Here lies the reason why we use the extra machinery of cotangent vectors, duality pairings, etc. Ideally, we would like to define  $\delta E$  to be the gradient w.r.t. the ‘flat  $L^2$ ’ metric on  $\mathcal{M}$ :  $\mathbf{g}_q^{L^2}(m, m') := \int m(x) m'(x) dx$ . (This is precisely what we do in Euclidean spaces, only w.r.t. the Euclidean metric.) However, doing so would require replacing  $\delta E(\theta, q)$  with  $\delta E(\theta, q) - \int \delta E(\theta, q) dx$  so that it lies in the tangent space (all tangent vectors must have zero mass). But the integral will not be well-defined in most cases and we hit a wall.

<sup>4</sup>The  $o(t)$  term in  $\ell(\theta + t\tau, x)$ 's expansion depends on  $x$ . Hence, to rigorously derive the ensuing expansion for  $F(\theta, t + \tau, q)$ , we require conditions on  $\ell$  and/or  $q$  guaranteeing that  $\int o(t, x) q(x) dx = o(t)$ . We abstain from explicitly stating such conditions to not complicate the exposition.

**The direction of maximum ascent.** To gain some intuition regarding what we actually do by ‘taking a step in the direction of  $\nabla^g E(\theta, q)$ ’, note that, for sufficiently regular functionals  $E$ ,

$$E(\theta + \tau, q + m) \approx E(\theta, q) + \langle (\tau, m), \delta E(\theta, q) \rangle = E(\theta, q) + g_{(\theta, q)}((\tau, m), \nabla^g E(\theta, q)) \quad (26)$$

for any given point  $(\theta, q)$  in  $\mathcal{M}$  and ‘small’ tangent vectors  $(\tau, m)$  in  $\mathcal{TM}$ , with the equality holding exactly in the limit as “ $(\tau, m)$ ’s size tends to zero”. To quantify “ $(\tau, m)$ ’s size” we use the norm on  $\mathcal{TM}$  induced by our metric:

$$\|(\tau, m)\|_{(\theta, q)}^g := g_{(\theta, q)}((\tau, m), (\tau, m)).$$

Armed with the above, we can then ask ‘out of all tangent vectors  $(\tau, m)$  of size  $\varepsilon$ , which lead to the greatest increase in  $E$  at  $(\theta, q)$ ’. That is, which  $(\tau^*, m^*)$  solve

$$\max_{\|(\tau, m)\|_{(\theta, q)}^g = \varepsilon} E(\theta + \tau, q + m)?$$

Were we to swap  $E(\theta + \tau, q + m)$  in the above with its approximation in (26), the Cauchy–Schwarz inequality would then tell us that  $(\tau^*, m^*)$  equals the (appropriately rescaled) gradient  $\varepsilon \nabla^g E(\theta, q) / \|\nabla^g E(\theta, q)\|_{(\theta, q)}^g$ :

$$\arg \max_{\|(\tau, m)\|_{(\theta, q)}^g = \varepsilon} E(\theta + \tau, q + m) \approx \arg \max_{\|(\tau, m)\|_{(\theta, q)}^g = \varepsilon} g_{(\theta, q)}((\tau, m), \nabla^g E(\theta, q)) = \frac{\varepsilon \nabla^g E(\theta, q)}{\|\nabla^g E(\theta, q)\|_{(\theta, q)}^g}.$$

Assuming that the above equality holds exactly as  $\varepsilon \rightarrow 0$ , we find that  $\nabla^g E(\theta, q)$  points in the direction of steepest ascent for  $E$  at  $(\theta, q)$  in the geometry defined by  $g$  (that is, using the norm induced by  $g$  to measure the length of vectors).

**Maximizing quadratic functionals.** We are now faced with the question ‘which geometry or metric  $g$  should we use to define gradients or directions of maximum ascent?’. While in practice this question often gets usurped by the more pragmatic ‘which geometries lead to gradient flows that can be efficiently approximated?’, considering which geometries are most attractive, even if only in a theoretical sense, still proves insightful. A straightforward way to approach this question is noting that (21) implies that  $\nabla^g E(\theta, q)$  solves

$$G_{\theta, q}(\tau, m) = \delta E(\theta, q).$$

It follows that  $(\theta, q) + \nabla_{(\theta, q)}^g E(\theta, q)$  maximizes a quadratic approximation to  $E$  around  $(\theta, q)$ :

$$\nabla^g E(\theta, q) = \arg \max_{(\tau, m) \in \mathcal{TM}} \left\{ E(\theta, q) + \langle (\tau, m), \delta E(\theta, q) \rangle - \frac{1}{2} \langle G_{\theta, q}(\tau, m), (\tau, m) \rangle \right\}. \quad (27)$$

From this vantage point, it seems natural to pick  $G$  so that the objective in (27) closely approximates  $E$  around  $(\theta, q)$ . We revisit this point for the free energy  $F$  in App. B.2

## B The three flows

Throughout the following, we assume that the reader is acquainted with the contents of App. A.

### B.1 The gradient flow (Sect. 2.1)

Here, we use the geometry on  $\mathcal{M} = \Theta \times \mathcal{P}(\mathcal{X})$  which leads to the gradient flow with the cheapest and most straightforward approximations that we know of (e.g. compare with the geometries in [42, 31], analogously extended from  $\mathcal{P}(\mathcal{X})$  to  $\mathcal{M}$ ): the one obtained as the product of the Euclidean geometry on  $\Theta$  and the Wasserstein-2 geometry on  $\mathcal{P}(\mathcal{X})$ . More formally, the geometry induced by the metric with block-diagonal tensor  $\text{diag}(\text{I}_{D_\theta}, \text{G}_q^W)$  (cf. App. A.2), where  $\text{I}_{D_\theta}$  denotes the identity operator on  $\mathcal{T}\Theta$  (i.e.  $\text{I}_{D_\theta} \tau = \tau$  for all  $\tau$  in  $\mathcal{T}\Theta$ ) and  $\text{G}_q^W$  the Wasserstein-2 tensor on  $\mathcal{P}(\mathcal{X})$  in (18). Combining Lem. 1 and (18,25) we find that  $F$ ’s gradient is given by (4), and its corresponding gradient flow by (5).

## B.2 The Newton flow and its approximations (Sect. 2.2)

### B.2.1 A differential-geometric perspective on Newton's method for maximizing functions on Euclidean spaces

Recall that Newton's method for maximizing a (say, twice-differentiable and strongly-concave) function  $f : \mathbb{R}^n \rightarrow \mathbb{R}$ ,

$$x_{k+1} = x_k + h[\mathcal{H}_f(x_k)]^{-1} \nabla_x f(x_k) \quad \forall k = 1, 2, \dots,$$

is the Euler discretization of the *Newton flow*:

$$\dot{x}_t = [\mathcal{H}_f(x_t)]^{-1} \nabla_x f(x_t) \quad \forall t \geq 0, \quad (28)$$

where  $\mathcal{H}_f = -(\partial^2 f / \partial x_i \partial x_j)_{i,j=1}^n$  denotes  $f$ 's negative Hessian. At each point in time  $t$ , the flow follows the *Newton direction*  $v_N(x) := [\mathcal{H}_f(x)]^{-1} \nabla_x f(x)$  at  $x_t$  (i.e. with  $x = x_t$ ). The appropriate analogue of (21) shows that  $v_N$  is precisely  $f$ 's gradient  $\nabla^{g^N} f$  w.r.t. the Riemmanian metric  $g^N$  associated with the tensor  $(\mathcal{H}_f(x))_{x \in \mathbb{R}^n}$ . This is an appealing choice because the geometry induced by  $g^N$  on  $\mathbb{R}^n$  makes  $f$  isotropic, at least to second order:

$$\begin{aligned} f(x + tv) &= f(x) + t \langle \nabla_x f(x), v \rangle - \frac{t^2}{2} \langle \mathcal{H}_f v, v \rangle + o(t^2) \\ &= f(x) + t g^N(\nabla^{g^N} f(x), v) - \frac{t^2}{2} g_x^N(v, v) + o(t^2), \end{aligned} \quad (29)$$

by Taylor's Theorem. In other words, by replacing  $\nabla_x$  with  $\nabla^{g^N}$  we mitigate bad conditioning in  $f$  which, for the reasons discussed in [8, Secs. 9.4.4, 9.5.1] and illustrated in [8, Figs. 9.14, 9.15], generally makes  $v_N(x)$  a much better update direction than the Euclidean gradient  $\nabla_x f(x)$ . In what follows, we derive the analogue of the Newton direction for the free energy  $F$ . Doing so requires identifying an appropriate notion for  $F$ 's (negative) Hessian, which we achieve using an expansion of the form in (29).

### B.2.2 A second order Taylor expansion for $F$

By definition,

$$\begin{aligned} F(\theta + t\tau, q + tm) &= \int \ell(\theta + t\tau, x)(q(x) + tm(x))dx \\ &\quad - \int \log(q(x) + tm(x))(q(x) + tm(x))dx. \end{aligned}$$

But  $\log(z + t)(z + t) = \log(z)z + [\log(z) + 1]t + t^2/(2z) + o(t^2)$  and, so,

$$\begin{aligned} \int \log(q(x) + tm(x))(q(x) + tm(x))dx &= \int \log(q(x))q(x)dx + t \int \log(q(x))m(x)dx \\ &\quad + \frac{t^2}{2} \int \left( \frac{m(x)}{q(x)} \right)^2 q(x)dx + o(t^2). \end{aligned} \quad (30)$$

(Here, we have used that  $\int m(x)dx = 0$  because  $m$  belongs to  $\mathcal{TP}(\mathcal{X})$ . Rigorously arguing the above requires considerations similar to those in Footnote 4.) Similarly,

$$\begin{aligned} \int \ell(\theta + t\tau, x)(q(x) + tm(x)) &= \int \log(p_\theta(x, y))q(x)dx + t \int \langle \nabla_\theta \ell(\theta, x), \tau \rangle q(x)dx \\ &\quad + t \int \log(p_\theta(x, y))m(x)dx - \frac{t^2}{2} \int \langle \tau, \mathcal{H}_\theta(x)\tau \rangle q(x)dx \\ &\quad + t^2 \int \langle \nabla_\theta \ell(\theta, x), \tau \rangle m(x)dx + o(t^2). \end{aligned}$$

Putting the above together with (30) and applying Lem. 1, we obtain that

$$F(\theta + t\tau, q + tm) = F(\theta, q) + t \langle (\tau, m), \delta F(\theta, q) \rangle - \frac{t^2}{2} \langle (\tau, m), \mathcal{H}_F(\theta, q)(\tau, m) \rangle + o(t^2). \quad (31)$$

where  $\mathcal{H}_F(\theta, q)$  denotes the linear map from  $\mathcal{TM}$  to  $\mathcal{T}^*\mathcal{M}$  defined by

$$\mathcal{H}_F(\theta, q)(\tau, m) = \left( \left[ \int \mathcal{H}_\theta(x) q(x) dx \right] \tau + \int \nabla_\theta \ell(\theta, x) m(x) dx, \langle \nabla_\theta \ell(\theta, \cdot), \tau \rangle - \frac{m}{q} \right). \quad (32)$$

A comparison of (29,31) seems to imply that  $\mathcal{H}_F(\theta, q)$  might be a sensible analogue for  $F$ 's negative Hessian. Alternatively, we may view  $\mathcal{H}_F(\theta, q)$  as the ‘matrix’

$$\mathcal{H}_F(\theta, q) := \begin{bmatrix} \int \mathcal{H}_\theta(x) q(x) dx & -\nabla_\theta \ell(\theta, \cdot) \\ -\nabla_\theta \ell(\theta, \cdot) & q^{-1} \end{bmatrix}. \quad (33)$$

### B.2.3 The Newton direction and flow, and tractable approximations thereof

Suppose that  $F$ 's negative Hessian operator,  $\mathcal{H}_F$  in (32), is invertible everywhere on  $\mathcal{M}$ . Just as for  $f$  in App. B.2.1, we set the Newton direction at  $(\theta, q)$  to be

$$(\tau_N, m_N)(\theta, q) := [\mathcal{H}_F(\theta, q)]^{-1} \delta F(\theta, q), \quad (34)$$

where  $\delta F$  denotes  $F$ 's first variation in Lem. 1. Alternatively, assuming further that  $\mathcal{H}_F$  is positive definite everywhere, we can view  $(\tau_N, m_N)$  as  $F$ 's gradient  $\nabla^{g^N} F$  with respect to the metric,

$$g_{(\theta, q)}^N((\tau, m), (\tau, m)) := \langle (\tau, m), \mathcal{H}_F(\theta, q)(\tau, m) \rangle,$$

which makes  $F$  isotropic, at least to second order: by (31),

$$F(\theta + t\tau, q + tm) = F(\theta, q) + t g_{(\theta, q)}^N(\tau, m) \nabla^{g^N} F(\theta, q) - \frac{t^2}{2} g_{(\theta, q)}^N((\tau, m), (\tau, m)) + o(t^2).$$

Unfortunately, we know of no closed-form expressions for  $(\tau_N, m_N)$  or computationally tractable approximations to the corresponding flow. However, it is straightforward to find approximations to  $\mathcal{H}_F$  that have both:

**Block diagonal approximations  $\mathcal{H}_F$  and quasi-Newton directions.** Consider the block-diagonal approximation to  $\mathcal{H}_F$  obtained by zeroing the off-diagonal blocks in (33):

$$\mathcal{H}_F(\theta, q) \approx \text{diag} \left( \int \mathcal{H}_\theta(x) q(x) dx, q^{-1} \right) =: \text{diag}(\mathbf{G}_{(\theta, q)}, \mathbf{G}_q^{FR}). \quad (35)$$

In other words,  $\mathbf{G}_q^{FR}$  is the Fisher-Rao tensor on  $\mathcal{P}(\mathcal{X})$  (cf. App. A.2), while  $\mathbf{G}_{(\theta, q)}$  is the tensor obtained by integrating the negative log-likelihood's  $\theta$ -Hessian w.r.t.  $q$ . Using (25) and Lem. 1, we find that the resulting ‘quasi-Newton’ direction  $(\tau_{QN}, m_{QN})$  equals

$$\begin{aligned} \tau_{QN}(\theta, q) &= \left[ \int \mathcal{H}_\theta(x) q(x) dx \right]^{-1} \int \nabla_\theta \ell(\theta, x) q(x) dx, \\ (m_{QN}(\theta, q))(x) &= q(x) \left[ \log \left( \frac{p_\theta(x, y)}{q(x)} \right) - \int \log \left( \frac{p_\theta(x, y)}{q(x)} \right) q(x) dx \right]; \end{aligned}$$

and the corresponding gradient flow reads

$$\dot{\theta}_t = \tau_{QN}(\theta_t, q_t) \quad \dot{q}_t = m_{QN}(\theta_t, q_t).$$

While it is likely possible that the above flow can be approximated computationally using techniques along the lines of those in [43, 72], this would require estimating the log-density  $\log(q(x))$  of particle approximations  $q$ , a complication we opted to avoid in this paper. Instead, we (crudely) further approximate (35) by replacing the Fisher-Rao block  $\mathbf{G}_q^{FR}$  with a Wasserstein-2 block  $\mathbf{G}_q^W$  (cf. App. A.2). The  $\tau_{QN}(\theta, q)$ -component of the quasi-Newton remains unchanged, the  $m_{QN}(\theta, q)$ -component is now given by  $-\nabla_x \cdot [q \nabla_x \log(p_\theta(\cdot, y)/q)]$ , and we obtain the flow in (14).



### B.3 The marginal gradient flow (Sect. 2.3)

Here, we use the Wasserstein-2 geometry on  $\mathcal{P}(\mathcal{X})$ : that induced by the Wasserstein-2 metric  $\mathbf{g}^W$  with tensor  $(\mathbf{G}_q^W)_{q \in \mathcal{P}(\mathcal{X})}$ , cf. App. A.2. As we will now show, the marginal objective  $F_*$ 's gradient w.r.t. to this metric is given by (16RHS), from which it follows that the corresponding gradient flow is (16LHS). Given (18), substituting  $\mathcal{P}(\mathcal{X})$  for  $\mathcal{M}$  in (21), we find that

$$\nabla^{\mathbf{g}^W} F_*(q) = -\nabla_x \cdot [q \nabla_x \delta F_*(q)],$$

where  $\delta F_*$  denotes  $F_*$ 's first variation (defined analogously to (22)). Hence, we need only show that  $\delta F_* = \log(p_{\theta_*(q)}(\cdot, y)/q)$  or, equivalently, that

$$F_*(q + tm) = F_*(q) + t \left\langle \log \left( \frac{p_{\theta_*(q)}(\cdot, y)}{q} \right), m \right\rangle + o(t). \quad (36)$$

To argue (36), we assume that  $\theta_* : \mathcal{P}(\mathcal{X}) \rightarrow \mathbb{R}$  defines a differentiable functional: for each  $q$  in  $\mathcal{P}(\mathcal{X})$  there exists a linear map  $D_q \theta_*$  from  $\mathcal{TP}(\mathcal{X})$  to  $\mathcal{T}\Theta$  satisfying

$$(D_q \theta_*)m = \lim_{t \rightarrow 0} \frac{\theta_*(q + tm) - \theta_*(q)}{t} \quad \forall m \in \mathcal{T}_q \mathcal{P}(\mathcal{X}).$$

Because, with  $\|\tau\|$  denoting the Euclidean norm of  $\tau := \theta_*(q + tm) - \theta_*(q)$ ,

$$\ell(\theta_*(q + tm), x) = \ell(\theta_*(q), x) + t \langle \tau, \nabla_\theta \ell(\theta_*(q), x) \rangle + o(\|\tau\|),$$

it follows from  $\theta_*$ 's differentiability that

$$\ell(\theta_*(q + tm), x) = \ell(\theta_*(q), x) + t \langle (D_q \theta_*)m, \nabla_\theta \ell(\theta_*(q), x) \rangle + o(t).$$

For this reason,

$$\begin{aligned} & \int \ell(\theta_*(q + tm), x)(q(x) + tm(x))dx \\ &= \int [\ell(\theta_*(q), x) + t \langle (D_q \theta_*)m, \nabla_\theta \ell(\theta_*(q), x) \rangle + o(t)] (q(x) + tm(x))dx \\ &= \int \ell(\theta_*(q), x)q(x)dx + t \int \ell(\theta_*(q), x)m(x)dx \\ & \quad + t \left\langle (D_q \theta_*)m, \int \nabla_\theta \ell(\theta_*(q), x)q(x)dx \right\rangle + o(t). \end{aligned} \quad (37)$$

(Rigorously arguing the above requires considerations similar to those in Footnote 4.) But, by definition,  $\theta_*(q)$  maximizes  $\theta \mapsto F(\theta, q)$ , and we have that

$$\int \nabla_\theta \ell(\theta_*(q), x)q(x)dx = \nabla_\theta F(\theta_*(q), q) = 0.$$

Given that  $F_*(q) = F(\theta_*(q), q)$ , combining the above with (30,37) then yields (36).

## C Proofs for Sect. 2

*Proof of Theorem 2.* Examining (4) we see that  $\nabla_q F(\theta, q) = 0$  if and only if  $q \propto p_\theta(\cdot, y)$ . Given that  $q$  is a probability distribution, it follows that  $\nabla_q F(\theta, q) = 0$  if and only if  $q = p_\theta(\cdot|y)$ . The result then follows from

$$\begin{aligned} \nabla_\theta p_\theta(y) &= \int \nabla_\theta p_\theta(x, y)dx = \int \nabla_\theta \ell(\theta, x)p_\theta(x, y)dx = p_\theta(y) \int \nabla_\theta \ell(\theta, x)p_\theta(x|y)dx \\ &= p_\theta(y) \nabla_\theta F(\theta, p_\theta(\cdot|y)). \end{aligned} \quad (38)$$

□

*Proof of Theorem 3.* Given Thrm. 2, we need only show that  $\nabla F(\theta, q) = 0$  if and only if  $\theta = \theta_*(q)$  and  $\nabla F_*(q) = 0$ . However, Assumpt. 2 implies that  $\nabla_\theta F(\theta, q) = 0$  if and only if  $\theta = \theta_*(q)$ . The result then follows because (16) implies that  $\nabla F_*(q) = 0$  if and only if  $q = p_{\theta_*(q)}(\cdot|y)$ . □

## D On the convergence of the gradient flow

As we will show below, if  $(\theta_t, q_t)_{t \geq 0}$  solves (5), then

$$I_t := \frac{dF(\theta_t, q_t)}{dt} = \|\dot{\theta}_t\|^2 + \int \|\nabla_x R_t(x)\|^2 q_t(x) dx \geq 0, \quad (39)$$

where  $R_t(x) := \log(p_{\theta_t}(x, y)/q_t(x))$  and  $\|\cdot\|$  denotes the Euclidean norm on  $\mathbb{R}^{D_\theta}$  or  $\mathbb{R}^{D_x}$ , as appropriate. In other words, the free energy is non-decreasing along (5)'s solutions:  $F(\theta_t, q_t) \geq F(\theta_0, q_0)$  for all  $t \geq 0$ . Moreover, because  $q \mapsto F(\theta, q)$  is maximized at  $p_\theta(\cdot|y)$  (Thrm. 1),

$$\log(p_{\theta_t}(y)) = \int \log\left(\frac{p_{\theta_t}(x, y)}{p_{\theta_t}(x|y)}\right) p_{\theta_t}(x|y) dx = F(\theta_t, p_{\theta_t}(\cdot|y)) \geq F(\theta_t, q_t) \geq F(\theta_0, q_0) \quad \forall t \geq 0;$$

and it follows from Assumpt. 1 that  $\{\theta_t\}_{t \geq 0}$  is relatively compact. Hence, an extension of LaSalle's principle along the lines of [12] should imply that, as  $t$  tends to infinity,  $(\theta_t, q_t)$  approaches the set of points that make (39)'s RHS vanish. But we can re-write the RHS as

$$g((\dot{\theta}_t, \dot{q}_t), (\dot{\theta}_t, \dot{q}_t)) = g(\nabla F(\theta_t, q_t), \nabla F(\theta_t, q_t)) \geq 0,$$

where  $g$  denotes the metric described in App. B.1 and  $\nabla$  the corresponding gradient (whose components are given by (4)). In other words,  $(\theta_t, q_t)$  approaches the set of pairs that make  $F$ 's gradient vanish. Thrm. 2 tells us that these pairs  $(\theta_*, q_*)$  are precisely those for which  $\theta_*$  is a stationary point of the marginal likelihood and  $q_*$  is its corresponding posterior  $p_{\theta_*}(\cdot|y)$ .

*Proof of (39).* Using the chain rule and integration by parts, we find that

$$\begin{aligned} \frac{d}{dt} \int \ell(\theta_t, x) q_t(x) dx &= \int \frac{d\ell(\theta_t, x)}{dt} q_t(x) dx + \int \ell(\theta_t, x) \dot{q}_t(x) dx \\ &= \int \langle \nabla_\theta \ell(\theta_t, x), \dot{\theta}_t \rangle q_t(x) dx - \int \ell(\theta_t, x) \nabla_x \cdot [q_t(x) \nabla_x R_t(x)] dx \\ &= \|\dot{\theta}_t\|^2 + \int \langle \nabla_x \ell(\theta_t, x), \nabla_x R_t(x) \rangle q_t(x) dx, \end{aligned}$$

and

$$\begin{aligned} \frac{d}{dt} \int \log(q_t(x)) q_t(x) dx &= \int [\log(q_t(x)) + 1] \dot{q}_t(x) dx = - \int [\log(q_t(x)) + 1] \nabla_x \cdot [q_t(x) \nabla_x R_t(x)] dx \\ &= \int \langle \nabla_x \log(q_t(x)), \nabla_x R_t(x) \rangle q_t(x) dx, \end{aligned}$$

where  $\langle \cdot, \cdot \rangle$  denotes the Euclidean inner product on  $\mathbb{R}^{D_\theta}$  or  $\mathbb{R}^{D_x}$ , as appropriate. Re-arranging, we obtain (39).  $\square$

It is straightforward to give a more complete argument in the case of models with sufficiently regular strongly log-concave densities. First, we show that, in these cases, the marginal likelihood has a unique maximizer:

**Theorem 4.** *Suppose that  $(\theta, x) \mapsto \ell(\theta, x)$  is twice continuously differentiable. Moreover, that  $\ell$  is strictly concave or, in other words, that its Hessian negative definite everywhere:*

$$\nabla^2 \ell(\theta, x) = \begin{bmatrix} \nabla_\theta^2 \ell(\theta, x) & \nabla_\theta \nabla_x \ell(\theta, x) \\ \nabla_x \nabla_\theta \ell(\theta, x) & \nabla_x^2 \ell(\theta, x) \end{bmatrix} \prec 0 \quad \forall \theta \in \Theta, \quad x \in \mathcal{X}. \quad (40)$$

*Then, the marginal likelihood  $\theta \mapsto p_\theta(y)$  has a unique maximizer and no other stationary point.*

*Proof.* Because  $\nabla_\theta p_\theta(y) = p_\theta(y) \nabla_\theta \log(p_\theta(y))$  and  $z \mapsto \log(z)$  is a strictly increasing function, it suffices to show that  $\theta \mapsto \log(p_\theta(y))$  is strictly concave. To this end, note that

$$\nabla_\theta^2 \log(p_\theta(y)) = \nabla_\theta \frac{\nabla_\theta p_\theta(y)}{p_\theta(y)} = \frac{\nabla_\theta^2 p_\theta(y)}{p_\theta(y)} - \frac{\nabla_\theta p_\theta(y) \otimes \nabla_\theta p_\theta(y)}{p_\theta(y)^2},$$

where  $v \otimes v' := (v_i v'_j)_{i,j=1}^{D_\theta}$  for any vectors  $v, v' \in \mathbb{R}^{D_\theta}$ . But,

$$\begin{aligned} \nabla_\theta p_\theta(y) &= \int \nabla_\theta p_\theta(x, y) dx = \int \nabla_\theta \ell(\theta, x) p_\theta(x, y) dx, \\ \nabla_\theta^2 p_\theta(y) &= \int \nabla_\theta^2 \ell(\theta, x) p_\theta(x, y) dx + \int \nabla_\theta \ell(\theta, x) \otimes \nabla_\theta p_\theta(x, y) dx \\ &= \int \nabla_\theta^2 \ell(\theta, x) p_\theta(x, y) dx + \int \nabla_\theta \ell(\theta, x) \otimes \nabla_\theta \ell(\theta, x) p_\theta(x, y) dx; \end{aligned}$$

and, so,

$$\nabla_\theta^2 \log(p_\theta(y)) = \int \nabla_\theta^2 \ell(\theta, x) p_\theta(x|y) dx + \Sigma(\theta),$$

where

$$\Sigma(\theta) := \int \nabla_\theta \ell(\theta, x) \otimes \nabla_\theta \ell(\theta, x) p_\theta(x|y) dx - \int \nabla_\theta \ell(\theta, x) p_\theta(x|y) dx \otimes \int \nabla_\theta \ell(\theta, x) p_\theta(x|y) dx.$$

By the Brascamp–Lieb concentration inequality [10, Thrm. 4.1],

$$\begin{aligned} \Sigma(\theta) &\preceq \int \nabla_\theta \nabla_x \ell(\theta, x) [-\nabla_x^2 \log(p_\theta(x|y))]^{-1} \nabla_x \nabla_\theta \ell(\theta, x) p_\theta(x|y) dx \\ &= - \int \nabla_\theta \nabla_x \ell(\theta, x) [\nabla_x^2 \ell(\theta, x)]^{-1} \nabla_x \nabla_\theta \ell(\theta, x) p_\theta(x|y) dx. \end{aligned}$$

In short,

$$\nabla_\theta^2 \log(p_\theta(y)) \preceq \int [\nabla_\theta^2 \ell(\theta, x) - \nabla_\theta \nabla_x \ell(\theta, x) [\nabla_x^2 \ell(\theta, x)]^{-1} \nabla_x \nabla_\theta \ell(\theta, x)] p_\theta(x|y) dx.$$

The integrand is the Schur complement of  $\ell$ 's Hessian and, hence, negative definite for all  $(\theta, x)$ . Moreover, because  $\nabla_x^2 \ell$  is negative definite everywhere and  $\ell$  is twice-continuously differentiable, the integrand varies continuously in  $x$ ; whence it follows that the integral is negative definite for all  $\theta$ . In other words,  $\theta \mapsto \log(p_\theta(y))$  is strictly concave.  $\square$

If, furthermore, the density is strongly log-concave, the flow converges exponentially fast:

**Theorem 5.** *Suppose that the log likelihood  $\ell$  is twice continuously differentiable; strongly concave,*

$$\nabla^2 \ell(\theta, x) \preceq -\lambda I_{D_x + D_\theta} \quad \forall (\theta, x) \in \Theta \times \mathcal{X},$$

*for some  $\lambda > 0$ ; and has bounded  $\theta$ -gradient,*

$$\|\nabla_\theta \ell(\theta, x)\| \leq C \quad \forall (\theta, x) \in \Theta \times \mathcal{X},$$

*for some  $C > 0$ . Then, the marginal likelihood has a unique maximizer  $\theta_*$  and, if  $I_0 < \infty$ ,*

$$\|\theta_t - \theta_*\| \leq C' e^{-\lambda t} \quad \text{and} \quad \|q_t - p_{\theta_*}(\cdot|y)\|_{L^1} \leq C' e^{-\lambda t}, \quad \forall t \geq 0,$$

*for some  $C' > 0$ , where  $\|\cdot\|$  denotes the Euclidean norm on  $\mathbb{R}^{D_\theta}$  and  $\|\cdot\|_{L^1}$  the  $L^1$  norm on  $\mathcal{P}(\mathcal{X})$  (recall that we are conflating  $\mathcal{P}(\mathcal{X})$  with its subset of distributions with positive densities w.r.t. the Lebesgue measure and identifying each distribution with its density).*

*Proof.* As we will show below,

$$\frac{dI_t}{dt} \leq -2\lambda I_t; \quad (41)$$

from which it follows that  $I_t \leq e^{-2\lambda t} I_0$ . Hence,

$$\int_0^\infty \|\dot{\theta}_t\| dt \leq \int_0^\infty e^{-\lambda t} \sqrt{I_0} dt = \frac{\sqrt{I_0}}{\lambda}.$$

Thus,  $\theta_\infty := \int_0^\infty \dot{\theta}_t dt$  is well-defined and  $\theta_t$  converges to  $\theta_\infty$  exponentially fast:

$$\|\theta_\infty - \theta_t\| \leq \left\| \int_t^\infty \dot{\theta}_s ds \right\| \leq \int_t^\infty \|\dot{\theta}_s\| ds \leq \frac{\sqrt{I_0}}{\lambda} e^{-\lambda t}.$$

Next, using the fact that  $\log(p_{\theta_t}(x|y)/q_t(x)) = R_t - \log(p_{\theta_t}(y))$ , we find that

$$\int \|\nabla_x R_t(x)\|^2 q_t(x) dx = \int \left\| \nabla_x \log \left( \frac{p_{\theta_t}(x|y)}{q_t(x)} \right) \right\|^2 q_t(x) dx.$$

Because  $\nabla_x^2 \log(p_{\theta_t}(x|y)) = \nabla_x^2 \ell(\theta_t, x) \preceq -\lambda I_{D_x}$  for all  $t \geq 0$ , a logarithmic Sobolev inequality and the Csiszár-Kullback-Pinsker inequality, Thrm. 1 and (12) in [45] respectively, then imply that

$$\frac{1}{2} \|q_t - p_{\theta_t}(\cdot|y)\|_{L^1}^2 \leq KL(q_t \|p_{\theta_t}(\cdot|y)\|) \leq \int \|\nabla_x R_t(x)\|^2 q_t(x) dx \leq e^{-2\lambda t} I_0.$$

As we will show below, the boundedness assumption on  $\ell$ 's  $\theta$ -gradient implies that  $\theta \mapsto p_\theta(\cdot|y)$  is a Lipschitz map from  $(\Theta, \|\cdot\|)$  to  $(\mathcal{P}(\mathcal{X}), \|\cdot\|_{L^1})$ :

$$\|p_\theta(\cdot|y) - p_{\theta'}(\cdot|y)\| \leq 2C \|\theta - \theta'\|. \quad (42)$$

Applying the triangle inequality we then find that  $q_t$  converges exponentially fast to  $p_{\theta_\infty}(\cdot|y)$ :

$$\begin{aligned} \|q_t - p_{\theta_\infty}(\cdot|y)\|_{L^1} &\leq \|p_{\theta_t}(\cdot|y) - p_{\theta_\infty}(\cdot|y)\|_{L^1} + \|q_t - p_{\theta_t}(\cdot|y)\|_{L^1} \leq 2C \|\theta_t - \theta_\infty\| + \sqrt{2I_0} e^{-\lambda t} \\ &\leq (2C + \sqrt{2}) \sqrt{I_0} e^{-\lambda t}. \end{aligned}$$

Given Thrm. 4, the only thing we have left to do is argue that the limit  $\theta_\infty$  is a stationary point of the marginal likelihood. This follows from (38), the bounded convergence theorem, and our assumption that  $\nabla_\theta \ell$  is bounded:

$$\begin{aligned} \frac{\nabla_\theta p_{\theta_\infty}(y)}{p_{\theta_\infty}(y)} &= \int \nabla_\theta \ell(\theta_\infty, x) p_{\theta_\infty}(x|y) dx = \lim_{n \rightarrow \infty} \int \nabla_\theta \ell(\theta_n, x) p_{\theta_n}(x|y) dx \\ &= \lim_{n \rightarrow \infty} \left[ \dot{\theta}_n + \int \nabla_\theta \ell(\theta_n, x) [p_{\theta_n}(x|y) - q_n(x)] dx \right] = 0. \end{aligned}$$

□

*Proof of (41).* Here, we adapt the arguments in [45, Sec. 5] and [3, Sec. 2.3]. Let's start:  $(d\|\dot{\theta}_t\|^2/dt) = 2\langle \dot{\theta}_t, \ddot{\theta}_t \rangle$  and, using the notation introduced in (40),

$$\begin{aligned} \ddot{\theta}_t &= \frac{d}{dt} \dot{\theta}_t = \frac{d}{dt} \int \nabla_\theta \ell(\theta_t, x) q_t(x) dx = \int \left[ \frac{d}{dt} \nabla_\theta \ell(\theta_t, x) \right] q_t(x) dx + \int \nabla_\theta \ell(\theta_t, x) \dot{q}_t(x) dx \\ &= \int \nabla_\theta^2 \ell(\theta_t, x) \dot{\theta}_t q_t(x) dx - \int \nabla_\theta \ell(\theta_t, x) \nabla_x \cdot [q_t(x) \nabla_x R_t(x)] dx \\ &= \int \nabla_\theta^2 \ell(\theta_t, x) \dot{\theta}_t q_t(x) dx + \int [\nabla_\theta \nabla_x \ell(\theta_t, x)] \nabla_x R_t(x) q_t(x) dx, \end{aligned}$$

where the last equality follows from integration by parts. Hence,

$$\frac{d}{dt} \|\dot{\theta}_t\|^2 = 2 \int \left[ \left\langle \dot{\theta}_t, \nabla_\theta^2 \ell(\theta_t, x) \dot{\theta}_t \right\rangle + \left\langle \dot{\theta}_t, [\nabla_\theta \nabla_x \ell(\theta_t, x)] \nabla_x R_t(x) \right\rangle \right] q_t(x) dx. \quad (43)$$

Similarly,

$$\frac{d}{dt} \int \|R_t(x)\|^2 q_t(x) dx = \int \left[ \frac{d}{dt} \|\nabla_x R_t(x)\|^2 \right] q_t(x) dx + \int \|\nabla_x R_t(x)\|^2 \dot{q}_t(x) dx.$$

But, with  $l_t(x) := \log(q_t(x))$ ,

$$\begin{aligned} \frac{d}{dt} \nabla_x R_t(x) &= \frac{d}{dt} \nabla_x \ell(\theta_t, x) - \frac{d}{dt} \nabla_x l_t(x) = [\nabla_x \nabla_\theta \ell(\theta_t, x)] \dot{\theta}_t - \nabla_x \frac{d}{dt} l_t(x), \\ \Rightarrow \frac{d}{dt} \|\nabla_x R_t(x)\|^2 &= 2 \left\langle \nabla_x R_t(x), \frac{d}{dt} \nabla_x R_t(x) \right\rangle \\ &= 2 \left\langle \nabla_x R_t(x), [\nabla_x \nabla_\theta \ell(\theta_t, x)] \dot{\theta}_t \right\rangle - 2 \left\langle \nabla_x R_t(x), \nabla_x \frac{d}{dt} l_t(x) \right\rangle, \\ \Rightarrow \int \left[ \frac{d}{dt} \|\nabla_x R_t(x)\|^2 \right] q_t(x) dx &= 2 \int \left[ \left\langle \nabla_x R_t(x), [\nabla_x \nabla_\theta \ell(\theta_t, x)] \dot{\theta}_t \right\rangle - \left\langle \nabla_x R_t(x), \nabla_x \frac{d}{dt} l_t(x) \right\rangle \right] q_t(x) dx; \end{aligned}$$

and

$$\begin{aligned} \int \|\nabla_x R_t(x)\|^2 \dot{q}_t(x) dx &= \int \left\langle \nabla_x \|\nabla_x R_t(x)\|^2, \nabla_x R_t(x) \right\rangle q_t(x) dx \\ &= 2 \int \left\langle \nabla_x R_t(x), \nabla_x^2 R_t(x) \nabla_x R_t(x) \right\rangle q_t(x) dx \\ &= 2 \int \left[ \left\langle \nabla_x R_t(x), \nabla_x^2 \ell(\theta_t, x) \nabla_x R_t(x) \right\rangle - \left\langle \nabla_x R_t(x), \nabla_x^2 l_t(x) \nabla_x R_t(x) \right\rangle \right] q_t(x) dx. \end{aligned}$$

Putting the above together, we find that

$$\begin{aligned} \frac{dI_t}{dt} &= 2 \int \left\langle (\dot{\theta}_t, \nabla_x R_t(x)), \nabla^2 \ell(\theta_t, x) (\dot{\theta}_t, \nabla_x R_t(x)) \right\rangle q_t(x) dx \\ &\quad - 2 \int \left\langle \nabla_x R_t(x), \nabla_x \frac{d}{dt} l_t(x) + \nabla_x^2 l_t(x) \nabla_x R_t(x) \right\rangle q_t(x) dx \\ &\leq -2\lambda I_t - 2 \int \left\langle \nabla_x R_t(x), \nabla_x \frac{d}{dt} l_t(x) + \nabla_x^2 l_t(x) \nabla_x R_t(x) \right\rangle q_t(x) dx =: -2\lambda I_t - 2A. \end{aligned}$$

(The inequality follows from our assumption that  $(\theta, x) \mapsto p_\theta(x, y)$  is  $\lambda$ -strongly log-concave.) We now need to show that  $A$  is no greater than zero. To this end, note that

$$\begin{aligned} \frac{d}{dt} l_t(x) &= \frac{\dot{q}_t(x)}{q_t(x)} = -\frac{\nabla_x \cdot [q_t(x) \nabla_x R_t(x)]}{q_t(x)} = -\frac{\langle \nabla_x q_t(x), \nabla_x R_t(x) \rangle}{q_t(x)} - \Delta_x R_t(x) \\ &= -\langle \nabla_x l_t(x), \nabla_x R_t(x) \rangle - \Delta_x R_t(x), \end{aligned}$$

where  $\Delta_x$  denotes the Laplacian operator; from which it follows that

$$\nabla_x \frac{d}{dt} l_t(x) = -\nabla_x^2 l_t(x) \nabla_x R_t(x) - \nabla_x^2 R_t(x) \nabla_x l_t(x) - \nabla_x \Delta_x R_t(x).$$

Bochner's formula tells us that

$$-\langle \nabla_x R_t(x), \nabla_x \Delta_x R_t(x) \rangle = \text{tr}([\nabla_x^2 R_t(x)]^T \nabla_x^2 R_t(x)) - \frac{1}{2} \Delta_x \|\nabla_x R_t(x)\|^2,$$

where  $\text{tr}(\cdot)$  denotes the trace operator. But

$$\begin{aligned} -\frac{1}{2} \int q_t(x) \Delta_x \|\nabla_x R_t(x)\|^2 dx &= \frac{1}{2} \int \left\langle \nabla_x q_t(x), \nabla_x \|\nabla_x R_t(x)\|^2 \right\rangle dx \\ &= \int \left\langle \nabla_x q_t(x), \nabla_x^2 R_t(x) \nabla_x R_t(x) \right\rangle q_t(x) dx. \end{aligned}$$

Hence,

$$A = \int \text{tr}([\nabla_x^2 R_t(x)]^T \nabla_x^2 R_t(x)) q_t(x) dx \geq 0.$$

□

*Proof of (42).* The mean value theorem tells us that, for each  $\theta, \theta', x$ , there exists a  $\psi$  such that

$$|p_\theta(x|y) - p_{\theta'}(x|y)| = |\langle \theta - \theta', \nabla_\theta p_\psi(x|y) \rangle| \leq \|\theta - \theta'\| \|\nabla_\theta p_\psi(x|y)\|.$$

We will now show that  $\|\nabla_\theta p_\psi(x|y)\| \leq 2C p_\psi(x|y)$ , from which the claim will follow:

$$\int |p_\theta(x|y) - p_{\theta'}(x|y)| dx \leq \|\theta - \theta'\| \int \|\nabla_\theta p_\psi(x|y)\| dx \leq 2C \|\theta - \theta'\|.$$

To obtain  $\|\nabla_\theta p_\psi(x|y)\| \leq 2C p_\psi(x|y)$ , note that

$$\begin{aligned} \nabla_\psi p_\psi(x|y) &= \frac{\nabla_\theta p_\psi(x, y)}{p_\psi(y)} - \frac{\nabla_\theta p_\psi(y)}{p_\psi(y)} \frac{p_\psi(x, y)}{p_\psi(y)} \\ &= \left[ \nabla_\theta \ell(\psi, x) - \int \nabla_\theta \ell(\psi, x') p_\psi(x'|y) dx' \right] p_\psi(x|y). \end{aligned}$$

But,

$$\begin{aligned} \left\| \nabla_\theta \ell(\psi, x) - \int \nabla_\theta \ell(\psi, x') p_\psi(x'|y) dx' \right\| &\leq \|\nabla_\theta \ell(\psi, x)\| + \left\| \int \nabla_\theta \ell(\psi, x') p_\psi(x'|y) dx' \right\| \\ &\leq C + \int \|\nabla_\theta \ell(\psi, x')\| p_\psi(x'|y) dx' \leq 2C. \end{aligned}$$

□

## E Particle approximations to the quasi-Newton and marginal gradient flows

### E.1 Particle approximations to the quasi-Newton flow (Sec. 2.2)

The flow (14) is satisfied by the law of the following McKean-Vlasov SDE:

$$d\theta_t = \left[ \int \mathcal{H}_{\theta_t}(x) q_t(x) dx \right]^{-1} \left[ \int \nabla_\theta \ell(\theta_t, x) q_t(x) dx \right] dt, \quad dX_t = \nabla_x \ell(\theta_t, X_t) dt + \sqrt{2} dW_t, \quad (44)$$

where  $q_t$  denotes  $X_t$ 's law and  $(W_t)_{t \geq 0}$  a standard Brownian motion. We obtain (13) by following the same steps as in Sec. 2.1, only with (44) replacing (6) and an extra approximation in (8):

$$\left[ \int \mathcal{H}_{\theta_t}(x) q_t(x) dx \right]^{-1} \approx \left[ \frac{1}{N} \sum_{n=1}^N \mathcal{H}_{\theta_t}(X_t^n) \right]^{-1}.$$



## E.2 Particle approximations to the marginal gradient flow (Sec. 2.1)

The flow (16) is satisfied by the law of the following McKean-Vlasov SDE:

$$dX_t = \nabla_x \ell(\theta_*(q_t), X_t) dt + \sqrt{2} dW_t, \quad (45)$$

where  $q_t$  denotes  $X_t$ 's law and  $(W_t)_{t \geq 0}$  a standard Brownian motion. We obtain (15) by following the same steps as in Sec. 2.1, only with (45) substituting (6) and the approximations in (8) replaced by

$$q_t \approx \frac{1}{N} \sum_{n=1}^N \delta_{X_t^n} \Rightarrow \theta_*(q_t) \approx \theta_* \left( \frac{1}{N} \sum_{n=1}^N \delta_{X_t^n} \right).$$

## F Additional details for the numerical examples

### F.1 Toy hierarchical model

**Synthetic data.** We generate the data synthetically by sampling (11) with  $\theta$  set to 1.

**The marginal likelihood's global maximum and the corresponding posterior.** To obtain closed-form expressions for these, we rewrite the density (11) in matrix-vector notation:

$$p_\theta(x, y) = \mathcal{N}(y; x, I_{D_x}) \mathcal{N}(x; \theta \mathbf{1}_{D_x}, I_{D_x}) \quad \forall \theta \in \mathbb{R}, \quad x, y \in \mathbb{R}^{D_x}. \quad (46)$$

Combining the expressions in [6, p. 92] with the Sherman–Morrison formula, we then find that

$$p_\theta(y) = \mathcal{N}(y; \theta \mathbf{1}_{D_x}, 2I_{D_x}), \quad p_\theta(x|y) = \mathcal{N}\left(x; \frac{y + \theta \mathbf{1}_{D_x}}{2}, \frac{1}{2} I_{D_x}\right). \quad (47)$$

Because

$$\nabla_\theta \log(p_\theta(y)) = \mathbf{1}_{D_x}^T (y - \mathbf{1}_{D_x} \theta) = \mathbf{1}_{D_x}^T y - D_x \theta,$$

it follows the data's empirical mean is the marginal likelihood's unique maximizer  $\theta_*$ , and plugging it into (47) we obtain an expression for the corresponding posterior:

$$\theta_* = \frac{\mathbf{1}_{D_x}^T y}{D_x}, \quad p_{\theta_*}(x|y) = \mathcal{N}\left(x; \frac{1}{2} \left[ y + \frac{\mathbf{1}_{D_x}^T y}{D_x} \right], \frac{1}{2} I_{D_x}\right). \quad (48)$$

**Implementation details for PGA, PQN, and PMGA.** Taking derivatives of (46)'s log, we find that

$$\nabla_\theta \ell(\theta, x) = \mathbf{1}_{D_x}^T (x - \theta \mathbf{1}_{D_x}), \quad \mathcal{H}_\theta \equiv D_x, \quad \nabla_x \ell(\theta, x) = y - x - (x - \theta \mathbf{1}_{D_x}). \quad (49)$$

Given that

$$\nabla_\theta F(\theta, q) = \int \nabla_\theta \ell(\theta, x) q(x) dx = \mathbf{1}_{D_x}^T \left[ \int x q(x) dx - \theta \mathbf{1}_{D_x} \right], \quad (50)$$

Assumpt. 2 is satisfied with

$$\theta_*(q) = \frac{\mathbf{1}_{D_x}^T}{D_x} \int x q(x) dx \quad \forall q \in \mathcal{P}(\mathcal{X}) \Rightarrow \theta_*(x^{1:N}) = \frac{\mathbf{1}_{ND_x}^T x^{1:N}}{ND_x} \quad \forall x^{1:N} \in \mathcal{X}^N. \quad (51)$$

Given (49,51), PGA (9) then reads (52,53), PQN (9RHS,13) reads (53,54), and PMGA (15) reads (55):

$$\theta_{k+1} = \theta_k + h D_x [\theta_*(X_k^{1:N}) - \theta_k], \quad (52)$$

$$X_{k+1}^{1:N} = X_k^{1:N} + h [y^N + \theta_k \mathbf{1}_{ND_x} - 2X_k^{1:N}] + \sqrt{2h} W_k^{1:N}, \quad (53)$$

$$\theta_{k+1} = \theta_k + h [\theta_*(X_k^{1:N}) - \theta_k], \quad (54)$$

$$X_{k+1}^{1:N} = X_k^{1:N} + h [y^N + \theta_*(X_k^{1:N}) \mathbf{1}_{ND_x} - 2X_k^{1:N}] + \sqrt{2h} W_k^{1:N}, \quad (55)$$

where  $y^N$  stacks  $N$  copies of  $y$ ,  $X_k^{1:N} := (X_k^1, \dots, X_k^N)$ , and similarly for  $X_{k+1}^{1:N}$  and  $W_k^{1:N}$ . Lastly, because the  $\theta$ -gradient in (49) is a sum of  $D_x$  terms,  $\Lambda$  in (12) simply equals  $D_x^{-1}$  and the tweaked version of PGA (9RHS,12) coincides with PQN (53,54).

**Implementation details for EM.** Given (47,51), the EM steps read

$$(E) \quad q_{k+1} := \mathcal{N}\left(\frac{y + \theta_k \mathbf{1}_{D_x}}{2}, \frac{1}{2} I_{D_x}\right), \quad (M) \quad \theta_{k+1} := \frac{1}{2} \left( \frac{\mathbf{1}_{D_x}^T y}{D_x} + \theta_k \right).$$

## F.2 Bayesian logistic regression

**Dataset.** We use the Wisconsin Breast Cancer dataset  $\mathcal{Y}$ , created by Dr. William H. Wolberg [69] at the University of Wisconsin Hospitals, and freely available at

[https://archive.ics.uci.edu/ml/datasets/breast+cancer+wisconsin+\(original\)](https://archive.ics.uci.edu/ml/datasets/breast+cancer+wisconsin+(original)).

It contains 683 datapoints<sup>5</sup> each with nine features  $f \in \mathbb{R}^9$  extracted from a digitized image of a fine needle aspirate of a breast mass and an accompanying label  $l$  indicating whether the mass is benign ( $l = 0$ ) or malign ( $l = 1$ ). We normalize the features so that each has mean zero and unit standard deviation across the dataset. We split the dataset into 80/20 training and testing sets,  $\mathcal{Y}_{\text{train}}$  and  $\mathcal{Y}_{\text{test}}$ .

**Model.** We employ standard Bayesian logistic regression with Gaussian priors. That is, we assume that the datapoints' labels are conditionally independent given the features  $f$  and regression weights  $x \in \mathbb{R}^{D_x := 9}$ , each label with Bernoulli law and mean  $s(f^T x)$ , where  $s(z) := e^z / (1 + e^z)$  denotes the standard logistic function; and, following [20], we assign the prior  $\mathcal{N}(\theta \mathbf{1}_{D_x}, 5I_{D_x})$  to the weights  $x$ , where  $\theta$  denotes the (scalar) parameter to be estimated. The model's density is given by:

$$p_\theta(x, y_{\text{train}}) = \mathcal{N}(x; \theta \mathbf{1}_{D_x}, 5I_{D_x}) \prod_{(f,l) \in \mathcal{Y}_{\text{train}}} s(f^T x)^l [1 - s(f^T x)]^{1-l};$$

and it follows that

$$\ell(\theta, x) = \sum_{(f,l) \in \mathcal{Y}_{\text{train}}} [y f^T x - \log(1 + e^{f^T x})] - \frac{\|x - \mathbf{1}_{D_x} \theta\|^2}{5} \quad (56)$$

The marginal likelihood has a unique maximizer:

**Proposition 1.** *If  $f^T \mathbf{1}_{D_x} \neq 0$  for at least one  $(l, f)$  in  $\mathcal{Y}_{\text{train}}$ , then  $\theta \mapsto p_\theta(y_{\text{train}}) = \int p_\theta(x, y_{\text{train}}) dx$  has a single maximizer  $\theta_*$  and no other stationary points.*

*Proof.* Given Thrm. 4 in App. D, we need only argue that  $\ell$  is strictly concave. Taking gradients of (56), we find that

$$\nabla^2 \ell(\theta, x) = \frac{1}{5} \begin{bmatrix} -D_x & \mathbf{1}_{D_x}^T \\ \mathbf{1}_{D_x} & -I_{D_x} \end{bmatrix} - \sum_{(f,l) \in \mathcal{Y}_{\text{train}}} s(f^T x) [1 - s(f^T x)] f \otimes f.$$

The leftmost matrix has a single nonnegative eigenvalue. It equals zero, its geometric multiplicity is one, and its corresponding eigenvalue is the vector of ones  $\mathbf{1}_{D_x+1}$ . However,

$$v^T \left[ \sum_{(f,l) \in \mathcal{Y}_{\text{train}}} s(f^T x) [1 - s(f^T x)] f \otimes f \right] v = \sum_{(f,l) \in \mathcal{Y}_{\text{train}}} s(f^T x) [1 - s(f^T x)] (f^T v)^2 \geq 0$$

for all  $v$  in  $\mathbb{R}^{D_x}$ . By assumption,  $f^T \mathbf{1}_{D_x} \neq 0$  for at least one feature vector  $f$  in the test set, and the above inequality is strict if  $v = \mathbf{1}_{D_x}$ . It then follows that

$$z^T \nabla^2 \ell(\theta, x) z < 0 \quad \forall z \in \mathbb{R}^{D_x+1}, \quad \theta \in \Theta, \quad x \in \mathcal{X};$$

or, in other words, that  $\ell$  is strictly concave. □

<sup>5</sup>After removal of the 16 datapoints with missing features.

**Implementation details.** Taking gradients of (56), we obtain

$$\nabla_{\theta} \ell(\theta, x) = \frac{\mathbf{1}_{D_x}^T x - D_x \theta}{5}, \quad \mathcal{H}_{\theta} \equiv \frac{D_x}{5}, \quad \nabla_x \ell(\theta, x) = \frac{\theta \mathbf{1}_{D_x} - x}{5} + \sum_{(f,l) \in \mathcal{Y}_{\text{train}}} [l - s(f^T x)] f,$$

The same manipulations as in (50) show that Assumpt. 2 is satisfied with  $\theta_*(q)$  and  $\theta_*(x^{1:N})$  as in (51). Hence, PGA (9) reads (57,58), PQN (9RHS,13) reads (58,59), and PMGA (15) reads (60):

$$\theta_{k+1} = \theta_k + h(D_x/5)[\theta_*(X_k^{1:N}) - \theta_k], \quad (57)$$

$$X_{k+1}^n = X_k^n + h \left( \frac{\theta_k \mathbf{1}_{D_x} - X_k^n}{5} + \sum_{(f,l) \in \mathcal{Y}_{\text{train}}} [l - s(f^T X_k^n)] f \right) + \sqrt{2h} W_k^n \quad \forall n \in [N], \quad (58)$$

$$\theta_{k+1} = \theta_k + h[\theta_*(X_k^{1:N}) - \theta_k], \quad (59)$$

$$X_{k+1}^n = X_k^n + h \left( \frac{\theta_*(X_k^{1:N}) \mathbf{1}_{D_x} - X_k^n}{5} + \sum_{(f,l) \in \mathcal{Y}_{\text{train}}} [l - s(f^T X_k^n)] f \right) + \sqrt{2h} W_k^n \quad \forall n \in [N]. \quad (60)$$

Lastly, the SOUL algorithm (9LHS,17) reads (57),  $X_{k+1}^0 = X_k^N$ , and

$$X_{k+1}^{n+1} = X_{k+1}^n + h \left( \frac{\theta_k \mathbf{1}_{D_x} - X_{k+1}^n}{5} + \sum_{(f,l) \in \mathcal{Y}_{\text{train}}} [l - s(f^T X_{k+1}^n)] f \right) + \sqrt{2h} W_{k+1}^n \quad \forall n \in [N-1].$$

**Predictive performance metrics.** Given a new feature vector  $\hat{f}$ , we would ideally predict its label  $\hat{l}$  using the posterior predictive distribution associated with the marginal likelihood's maximizer  $\theta_*$ . In other words, using

$$p_{\theta_*}(\hat{l}|\hat{f}, y_{\text{train}}) = \int p(\hat{l}|\hat{f}, x) p_{\theta_*}(x|y_{\text{train}}) dx = \int s(\hat{f}^T x)^{\hat{l}} [1 - s(\hat{f}^T x)]^{1-\hat{l}} p_{\theta_*}(x|y_{\text{train}}) dx.$$

However,  $p_{\theta_*}(x|y_{\text{train}})$  is unknown. So, we replace it with a particle approximation  $q = M^{-1} \sum_{m=1}^M \delta_{Z^m}$  thereof obtained using PGA, PQN, PMGA, or SOUL:

$$\begin{aligned} p_{\theta_*}(\hat{l}|\hat{f}, y_{\text{train}}) &\approx \int s(\hat{f}^T x)^{\hat{l}} [1 - s(\hat{f}^T x)]^{1-\hat{l}} q(dx) \\ &= \frac{1}{M} \sum_{m=1}^M s(\hat{f}^T Z^m)^{\hat{l}} [1 - s(\hat{f}^T Z^m)]^{1-\hat{l}} =: g(\hat{l}|\hat{f}). \end{aligned} \quad (61)$$

We use two metrics to evaluate the approximation's predictive power. First, the average classification error over the test set  $\mathcal{Y}_{\text{test}}$ , i.e. the fraction of mislabelled test points were we to assign to each of them the label maximizing (61)'s RHS:

$$\text{Error} := \frac{1}{|\mathcal{Y}_{\text{test}}|} \sum_{(f,l) \in \mathcal{Y}_{\text{test}}} |l - \hat{l}(f)|, \quad \text{where} \quad \hat{l}(f) := \arg \max_{\hat{l} \in \{0,1\}} g(\hat{l}|f). \quad (62)$$

The second metric is the so-called log pointwise predictive density (LPPD, e.g. [63]):

$$\text{LPPD} := \frac{1}{|\mathcal{Y}_{\text{test}}|} \sum_{(f,l) \in \mathcal{Y}_{\text{test}}} \log(g(l|f)). \quad (63)$$

Interest in this metric stems from the assumption that the data is drawn independently from a 'data-generating process'  $p(dl, df)$ , in which case, for large test sets,

$$\begin{aligned} \text{LPPD} &\approx \int \log(g(l|f)) p(dl, df) \\ &= \int \left[ \int \log \left( \frac{g(l|f)}{p(l|f)} \right) p(dl|f) \right] p(df) + \int \log(p(l|f)) p(dl, df) \\ &= - \int KL(g(\cdot|f) || p(\cdot|f)) p(df) + \int \log(p(l|f)) p(dl, df). \end{aligned}$$

In other words, the larger LPPD is, the smaller we can expect the mean KL divergence between our classifier  $g(l|f)$  and the optimal classifier  $p(l|f)$ .

**Further numerical results.** To investigate the algorithms’ performances, we ran them 100 times, each time using a different random 80/20 training/testing split of the data. In all runs we employed a step size of  $h = 0.01$  (which ensured that no algorithm was on the verge of becoming unstable while simultaneously not being excessively small),  $K = 400$  steps, and  $N = 1, 10, 100$  particles. Tab. 2 shows the obtained LPPDs (63), test errors (62), stationary empirical variances of the parameter estimates, and computation times. For the predictive performance metrics, we initialized the estimates and particles at zero (as in [20]) and used the time-averaged approximations  $\bar{q}_{400}$ , cf. (10), with a burn-in of  $k_b = 200$ . (Warm-starting did not lead to any improvements here.) By  $k = 200$ , the PQN parameter estimates have not yet reached the stationary phase (Fig. 3a). Hence, for the variance estimates, we warm-start the algorithms using a preliminary run of PGA (with  $K = 400$ ,  $h = 0.01$ , and a single particle  $N = 1$ ) and then compute the estimates using a full  $K = 400$  run of the corresponding algorithm.

Table 2: **Bayesian logistic regression.** See text in App. F.2 for details.

Alg.	LPPD ( $\times 10^{-2}$ )	Error (%)	Variance ( $\times 10^{-4}$ )	Time (s)
$N = 1$				
PGA	$-9.73 \pm 1.04$	$3.58 \pm 0.78$	$14.1 \pm 13.6$	$0.03 \pm 0.01$
PQN	$-9.65 \pm 0.87$	$3.54 \pm 0.77$	$7.33 \pm 6.63$	$0.03 \pm 0.00$
PMGA	$-9.61 \pm 0.86$	$3.56 \pm 0.69$	$106 \pm 36.7$	$0.03 \pm 0.00$
SOUL	$-9.73 \pm 0.94$	$3.53 \pm 0.72$	$11.7 \pm 10.7$	$0.03 \pm 0.00$
$N = 10$				
PGA	$-9.40 \pm 0.28$	$3.55 \pm 0.71$	$1.25 \pm 1.01$	$0.09 \pm 0.01$
PQN	$-9.41 \pm 0.27$	$3.49 \pm 0.66$	$0.72 \pm 0.73$	$0.09 \pm 0.00$
PGMA	$-9.48 \pm 0.27$	$3.65 \pm 0.64$	$10.7 \pm 4.38$	$0.09 \pm 0.01$
SOUL	$-9.41 \pm 0.27$	$3.60 \pm 0.60$	$2.78 \pm 2.23$	$0.25 \pm 0.01$
$N = 100$				
PGA	$-9.38 \pm 0.08$	$3.46 \pm 0.32$	$0.13 \pm 0.10$	$1.22 \pm 0.34$
PQN	$-9.41 \pm 0.09$	$3.47 \pm 0.33$	$0.06 \pm 0.06$	$1.17 \pm 0.26$
PMGA	$-9.39 \pm 0.07$	$3.44 \pm 0.33$	$1.03 \pm 0.35$	$1.15 \pm 0.18$
SOUL	$-9.39 \pm 0.09$	$3.43 \pm 0.35$	$0.28 \pm 0.61$	$13.4 \pm 0.23$

All four algorithms achieve similar predictive performances with very little gains as the particle number  $N$  is increased: it seems that the problem is straightforward and that a single particle in the vicinity of the optimal posteriors’s single mode (Fig. 3b) suffices for prediction. The variance of the stationary PGA, PQN, and PMGA’s estimates seems to decay linearly with  $N$ ; which is unsurprising given that these algorithms are Monte Carlo methods. Lastly, vectorizing the computations across particles in PGA, PQN, and PMGA makes them run faster than SOUL, and the gap in computation times widens as  $N$  is increased.

### F.3 Bayesian neural network

**Dataset.** We use the MNIST [41] dataset  $\mathcal{Y}$ , available under the terms of the Creative Commons Attribution-Share Alike 3.0 license at

<http://yann.lecun.com/exdb/mnist/>.

(Copyright held by Yann LeCun and Corinna Cortes.) It contains 70,000  $28 \times 28$  grayscale images  $f \in \mathbb{R}^{784}$  of handwritten digits each accompanied its corresponding label  $l$ . We avoid any big data issues by subsampling 1000 datapoints with labels 4 and 9 just as in [70] (except that we pick the labels 4 and 9 rather than 1 and 2 to make the problem more challenging). We normalize the 784 features so that each has mean zero and unit

standard deviation across the dataset. We split the dataset into 80/20 training and testing sets,  $\mathcal{Y}_{\text{train}}$  and  $\mathcal{Y}_{\text{test}}$ .

**Model.** Following [70], we employ a Bayesian two-layer neural network with tanh activation functions, a softmax output layer, and Gaussian priors on the weights (however, we simplify matters by setting all network biases to zero). That is, we assume that the datapoints' labels are conditionally independent given the features  $f$  and network weights  $x := (w, v)$  (where  $w \in \mathbb{R}^{D_w := 40 \times 784 = 31360}$  and  $w^0 \in \mathbb{R}^{D_v := 2 \times 40 = 80}$ ) with law

$$p(l|f, x) \propto \exp \left( \sum_{j=1}^{40} v_{lj} \tanh \left( \sum_{i=1}^{784} w_{ji} f_i \right) \right). \quad (64)$$

Also as in [70], we assign the prior  $\mathcal{N}(\mathbf{0}_{D_w}, e^{2\alpha} I_{D_w})$  to the input layer's weights  $w$  and  $\mathcal{N}(\mathbf{0}_{D_v}, e^{2\beta} I_{D_v})$  to those of the output layer, where  $\mathbf{0}_d$  denotes the  $d$ -dimensional vector of zeros. However, rather than assigning a hyperprior to  $\alpha, \beta$ , we instead learn them from the data (i.e.  $\theta := (\alpha, \beta)$ ). The model's density is given by:

$$p_\theta(x, y_{\text{train}}) = \mathcal{N}(w; \mathbf{0}_{D_w}, e^{2\alpha} I_{D_w}) \mathcal{N}(v; \mathbf{0}_{D_v}, e^{2\beta} I_{D_v}) \prod_{(f, l) \in \mathcal{Y}_{\text{train}}} p(l|f, x).$$

**Implementation details.** The necessary  $\theta$ -gradients and negative  $\theta$ -Hessian are straightforward to compute by hand:

$$\nabla_\theta \ell(\theta, x) = \begin{bmatrix} ||w||^2 e^{-2\alpha} - D_w \\ ||v||^2 e^{-2\beta} - D_v \end{bmatrix}, \quad \mathcal{H}_\theta(x) = \begin{bmatrix} 2||w||^2 e^{-2\alpha} & 0 \\ 0 & 2||v||^2 e^{-2\beta} \end{bmatrix}.$$

For the  $x$ -gradients, we use JAX's grad function (implementing a version of autograd). Given that

$$\nabla_\theta F(\theta, q) = \int \nabla_\theta \ell(\theta, x) q(x) dx = \begin{bmatrix} e^{-2\alpha} \int ||w||^2 q(w) dw - D_w \\ e^{-2\beta} \int ||v||^2 q(v) dv - D_v \end{bmatrix},$$

where  $q(w)$  and  $q(v)$  respectively denote  $q$ 's  $w$  and  $v$  marginals, Assumpt. 2 is satisfied with

$$\begin{aligned} \theta_*(q) &= \begin{bmatrix} \alpha_*(q) \\ \beta_*(q) \end{bmatrix} = \begin{bmatrix} \frac{1}{2} \log \left( D_w^{-1} \int ||w||^2 q(w) dw \right) \\ \frac{1}{2} \log \left( D_v^{-1} \int ||v||^2 q(v) dv \right) \end{bmatrix} \quad \forall q \in \mathcal{P}(\mathcal{X}), \\ \Rightarrow \theta_*(x^{1:N}) &= \begin{bmatrix} \alpha_*(x^{1:N}) \\ \beta_*(x^{1:N}) \end{bmatrix} = \begin{bmatrix} \frac{1}{2} \log \left( [ND_w]^{-1} \sum_{n=1}^N ||w^n||^2 \right) \\ \frac{1}{2} \log \left( [ND_v]^{-1} \sum_{n=1}^N ||v^n||^2 \right) \end{bmatrix} \quad \forall x^{1:N} = (w^{1:N}, v^{1:N}) \in \mathcal{X}^N. \end{aligned}$$

Implementing PGA, PQN, PMGA, and SOUL then consists of exploiting the above expressions and respectively running (9), (9RHS,13), (15), and (9LHS,17). To avoid any memory issues, we only store the current particle cloud and use its empirical distribution to approximate the posteriors (rather than a time-averaged version thereof). We initialize the parameter estimates at zero and the weights at samples drawn independently from the priors.

Given the high dimensionality of the latent variables, PGA and SOUL prove less stable than PQN and PMGA (the former loose stability around  $h \approx 10^{-4}$ , while the latter around  $h \approx 1$ ). Hence, we stabilize PGA and SOUL using the heuristic discussed in Sec. 2.1. This simply entails respectively dividing the  $\alpha$  and  $\beta$  gradients by  $D_w$  and  $D_v$ . We then set  $h := 0.1$  which ensures that no algorithm is close to losing stability.

**Predictive performance metrics.** We use the test error and log pointwise predictive density defined as in (62,63), only with the classifier  $g(l|f)$  now given by  $N^{-1} \sum_{n=1}^N p(l|f, X_K^n)$ , where  $p(l|f, x)$  is as in (64) and  $X_K^{1:N}$  denotes the final particle cloud produced PGA, PQN, PMGA, or SOUL.

## G The mean-field limits and the time-discrezation bias

The mean-field ( $N \rightarrow \infty$ ) limit of PGA (9) is (65,66), that of PQN (9RHS,13) is (66,67), and that of PMGA (15) is (68):

$$\theta_{k+1} = \theta_k + h \int \nabla_{\theta} \ell(\theta_k, x) q_k(x) dx, \quad (65)$$

$$X_{k+1} = X_k + h \nabla_x \ell(\theta_k, X_k) + \sqrt{2h} W_k, \quad (66)$$

$$\theta_{k+1} = \theta_k + h \left[ \int \mathcal{H}_{\theta}(x) q_k(x) dx \right]^{-1} \int \nabla_{\theta} \ell(\theta_k, x) q_k(x) dx, \quad (67)$$

$$X_{k+1} = X_k + h \nabla_x \ell(\theta_*(q_k), X_k) + \sqrt{2h} W_k. \quad (68)$$

where, in all three cases,  $q_k$  denotes  $X_k$ 's law and, in (68) we are assuming that Assumpt. 2 holds. We can re-write (65,67) as

$$\theta_{k+1} = u(\theta_k, q_k), \quad (69)$$

where  $u : \Theta \times \mathcal{P}(\mathcal{X}) \rightarrow \Theta$  denotes an ‘update’ operator satisfying

$$\forall q \in \mathcal{P}(\mathcal{X}), \quad \nabla_{\theta} F(\theta_*, q) = 0 \Rightarrow u(\theta_*, q) = \theta_*. \quad (70)$$

Now, (66,69)'s joint law  $q_k(d\theta, dx)$  satisfies

$$q_{k+1}(d\psi, dz) = \int_{\theta, x} q_k(d\theta, dx) \delta_{u(\theta, q_k)}(d\psi) K_{\theta}(x, dz), \quad (71)$$

where  $K_{\theta}$  denotes the ULA kernel:

$$K_{\theta}(x, dz) = K_{\theta}(x, z) dz := \mathcal{N}(z; x + h \nabla_x \ell(\theta, x), 2h I_{D_x}) dz \quad \forall x, z \in \mathcal{X}, \quad \theta \in \Theta. \quad (72)$$

What we would like is for

$$\pi(d\theta, dx) := \delta_{\theta_*}(d\theta) p_{\theta_*}(dx|y)$$

to be a fixed point of (71) whenever  $\theta_*$  is a maximizer of  $\theta \mapsto p_{\theta}(y)$  and  $p_{\theta_*}(dx|y)$  is the corresponding posterior. However, applying Thrm. 2 and (70), we find that

$$\begin{aligned} \int_{\theta, x} \pi(d\theta, dx) \delta_{u(\theta, \pi(dx))}(d\psi) K_{\theta}(x, dz) &= \int_{\theta, x} \delta_{\theta_*}(d\theta) p_{\theta_*}(dx|y) \delta_{u(\theta, p_{\theta_*}(dx|y))}(d\psi) K_{\theta}(x, dz) \\ &= \delta_{u(\theta_*, p_{\theta_*}(dx|y))}(d\psi) \int_x p_{\theta_*}(dx|y) K_{\theta_*}(x, dz) \\ &= \delta_{\theta_*}(d\psi) \int_x p_{\theta_*}(dx|y) K_{\theta_*}(x, dz). \end{aligned}$$

Hence,  $\pi$  is a fixed point of (71) if and only if  $p_{\theta_*}(dx|y)$  is a stationary distribution of  $K_{\theta_*}(x, dz)$ :

$$p_{\theta_*}(z|y) = \int p_{\theta_*}(x|y) K_{\theta_*}(x, z) dx \quad (73)$$

However, we know that this is not the case because the ULA kernel is biased, e.g. see [55].

The case of (68) is similar:  $q_k$  satisfies

$$q_{k+1}(z) = \int q_k(x) K_{\theta_*(q_k)}(x, z) dx.$$

Given that  $\theta_*(p_{\theta_*}(\cdot|y)) = \theta_*$  (Thrm. 2), we have that  $p_{\theta_*}(\cdot|y)$  is a fixed point of the above if and only if (73) holds, which it does not.

An obvious way to get (73) to hold is replacing the ULA kernel  $K_{\theta}$  with a kernel whose stationary distribution is the posterior  $p_{\theta}(\cdot|y)$  (e.g. by adding an accept-reject step to the ULA kernel). This removes the time-discretization bias in the mean-field regime. In App. I, we will see another (slightly less obvious) way to do so that also removes the bias for finite  $N$  (at least in the case of PMGA).



## G.1 Rates of convergence for Ex. 1

To investigate the rate of convergence of the three algorithms in the case of the toy hierarchical model (Ex. 1), we examine the mean-field limits (65–68) which respectively read:

$$\theta_{k+1} = \theta_k + hD_x[\nu_k - \theta_k], \quad (74)$$

$$X_{k+1} = X_k + h[y + \theta_k \mathbf{1}_{D_x} - 2X_k] + \sqrt{2h}W_k, \quad (75)$$

$$\theta_{k+1} = \theta_k + h[\nu_k - \theta_k], \quad (76)$$

$$X_{k+1} = X_k + h[y + \nu_k \mathbf{1}_{D_x} - 2X_k] + \sqrt{2h}W_k. \quad (77)$$

where, in all cases,  $\nu_k := \mathbb{E}[\mathbf{1}_{D_x}^T X_k / D_x]$  denotes the mean of the average of  $X_k$ 's components. Left-multiplying (75,77) by  $D_x^{-1} \mathbf{1}_{D_x}^T$  and taking expectations in, we respectively find that

$$\nu_{k+1} = \nu_k + h[\mathbf{1}_{D_x}^T y / D_x + \theta_k - 2\nu_k] \quad (78)$$

$$\nu_{k+1} = \nu_k + h[\mathbf{1}_{D_x}^T y / D_x - \nu_k]. \quad (79)$$

Note that both (74,78) and (76,78) have a unique fixed point  $(\theta_\infty, \nu_\infty)$  given by  $\theta_\infty = \nu_\infty = \theta_*$ , where  $\theta_* = \mathbf{1}_{D_x}^T y / D_x$  denotes the marginal likelihood's unique maximizer (cf. App. F.1). Re-writing (74,78) and (76,78) in matrix-vector notation,

$$\begin{aligned} \begin{bmatrix} \theta_{k+1} \\ \nu_{k+1} \end{bmatrix} &= A_h^G \begin{bmatrix} \theta_k \\ \nu_k \end{bmatrix} + \begin{bmatrix} 0 \\ h \mathbf{1}_{D_x}^T y / D_x \end{bmatrix} \quad \text{where} \quad A_h^G := \begin{bmatrix} 1 - hD_x & hD_x \\ h & 1 - 2h \end{bmatrix}, \\ \begin{bmatrix} \theta_{k+1} \\ \nu_{k+1} \end{bmatrix} &= A_h^N \begin{bmatrix} \theta_k \\ \nu_k \end{bmatrix} + \begin{bmatrix} 0 \\ h \mathbf{1}_{D_x}^T y / D_x \end{bmatrix} \quad \text{where} \quad A_h^N := \begin{bmatrix} 1 - h & h \\ h & 1 - 2h \end{bmatrix}, \end{aligned}$$

then clarifies that  $\theta_k$ 's speed of convergence to  $\theta_*$  is  $\mathcal{O}(\rho_{G,h}^k)$  in the case of (74,78) and  $\mathcal{O}(\rho_{N,h}^k)$  in that of (76,78), where  $\rho_{G,h}$  denotes  $A_h^G$ 's spectral radius and  $\rho_{N,h}$  denotes  $A_h^N$ 's. After some quick algebra, we find that

$$\rho_{G,h} = \max \left\{ \left| 1 - h \left( 1 + \frac{D_x}{2} \pm \frac{\sqrt{D_x^2 + 4}}{2} \right) \right| \right\}, \quad \rho_{N,h} = \max \left\{ \left| 1 - h \left( \frac{3}{2} \pm \frac{\sqrt{5}}{2} \right) \right| \right\}.$$

As for PMGA's mean-field limit (77), recall that we use  $\theta_*(q_k) = D_x^{-1} \mathbf{1}_{D_x}^T \int x q_k(x) dx = \nu_k$  to estimate  $\theta_*$ , where  $q_k$  denotes  $X_k$ 's law, and note that  $\nu_k$  in (79) converges to  $\theta_*$  at a rate of  $\mathcal{O}(\rho_{M,h}^k)$ , where  $\rho_{M,h} := |1 - h|$ . Two observations are in order:

- **Dependence on  $D_x$ .** In the case of PGA, the radius  $\rho_{G,h}$  depends on the dimension  $D_x$  of the latent space. For large dimensions,  $\rho_{G,h} \approx |1 - h(1 + D_x)|$  implying that PGA is stable only for small very small step sizes (roughly, those smaller than  $2/(1 + D_x)$ ), which explains the need for the tweak (12). On the other hand, the radii for PQN and PMGA are independent of  $D_x$ . For these reasons, tuning the step size for PGA proves challenging and delicately depends on  $D_x$ , while tuning it for PQN and PMGA is straightforward and does not require taking  $D_x$  into account.
- **Relative speeds.** For all step sizes,  $\rho_{G,h}$  and  $\rho_{N,h}$  are both bounded below by  $\rho_{M,h}$  (see Fig. 5), implying that PMGA always converges faster than PGA and PQN, at least in the mean-field regime. It is not necessarily the case that  $\rho_{N,h} \leq \rho_{G,h}$ : for small step sizes this fails to hold. However, the range of  $h$ s for which  $\rho_{N,h} > \rho_{G,h}$  decreases precipitously with the latent space dimension  $D_x$  (Fig. 5). Hence, we expect PQN to outperform PGA unless we are using very small step sizes (likely, those too small to achieve any reasonable speed of convergence).

Consider now the matter of choosing the step size  $h$  that achieves the fastest convergence for each algorithm. That is, the  $h$  that minimizes the corresponding radius. It is a simple matter to verify that

$$h_G = \frac{2}{2 + D_x}, \quad h_N = \frac{2}{3}, \quad h_M = 1, \quad \text{with} \quad \rho_G = \frac{\sqrt{D_x^2 + 4}}{D_x + 2}, \quad \rho_N = \frac{\sqrt{5}}{3}, \quad \rho_M = 0,$$

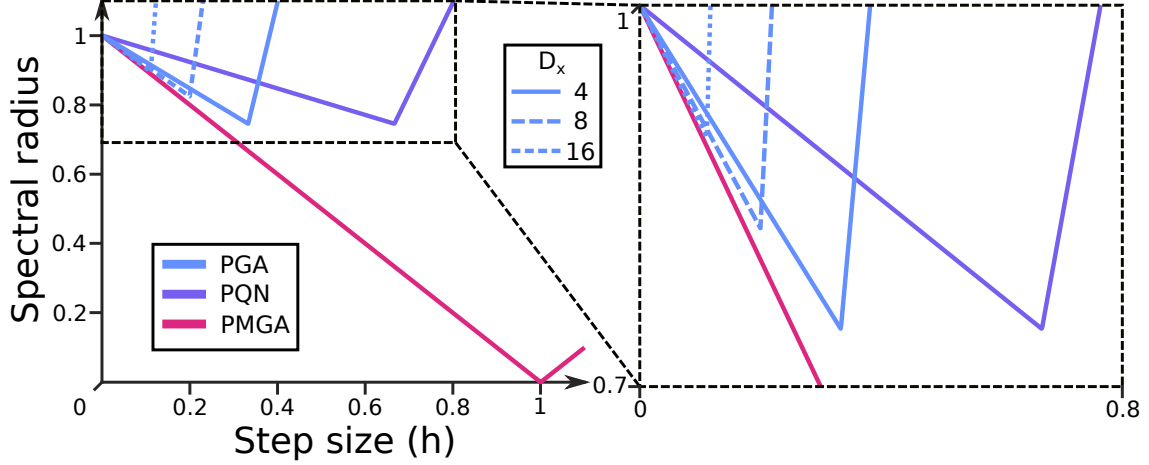


Figure 5: Spectral radii  $\rho_{G,h}$  (PGA),  $\rho_{N,h}$  (PQN), and  $\rho_{M,h}$  (PMGA) as a function of step size  $h$ .

where  $h_G, h_N, h_M$  respectively denote the optimal step sizes for PGA, PQN, and PMGA, and  $\rho_G, \rho_N, \rho_M$  the corresponding radii. Note that,  $\rho_G \geq \rho_N \geq \rho_M$  whenever  $D_x \geq 4$ . Hence, with the exception of very low dimensional cases, and with the step sizes well-tuned, PQN will outperform PGA. PMGA will always outperform either. Moreover,  $\rho_G \rightarrow 1$  as  $D_x \rightarrow \infty$  and, hence, PGA's speed of convergence degenerates with increasing latent space dimension regardless of the step size  $h$  that we use. That of PQN does not and, if we tune the algorithm well, will be  $\mathcal{O}([2/3]^k)$  for all  $D_x$ . Setting  $h := 1$  in (79), we find that, regardless of  $D_x$ , PMGA's parameter estimates will converge in a single step, at least in the mean-field regime. Of course, this fails to materialize when we run the algorithm in practice because the noise in (77) exacts an  $\mathcal{O}(1/\sqrt{KND_x})$  error in our time-averaged estimates, which is what we see in Fig. 1c (similar considerations also apply to PGA and PQN in stationarity). Lastly, we ought to mention that we have observed these behaviours replicated across other numerical experiments, hinting that they might hold more widely. However, until an analysis establishing so becomes available, we only count this as anecdotal evidence.

## H The continuum limits and the finite-population-size bias

For the sake of simplicity, suppose that Assumpt. 2 holds. The continuum limit ( $h \rightarrow 0$ ) of PGA (9) is (80,81), that of PQN (9RHS,13) is (81,82), and that of PMGA (15) is (83):

$$d\theta_t = \frac{1}{N} \left[ \sum_{n=1}^N \nabla_{\theta} \ell(\theta_t, X_t^n) \right] dt, \quad (80)$$

$$dX_t^n = \nabla_x \ell(\theta_t, X_t^n) dt + \sqrt{2} dW_t^n \quad \forall n \in [N], \quad (81)$$

$$d\theta_t = \left[ \sum_{n=1}^N \mathcal{H}_{\theta_t}(X_t^n) \right]^{-1} \left[ \sum_{n=1}^N \nabla_{\theta} \ell(\theta_t, X_t^n) \right] dt, \quad (82)$$

$$dX_t^n = \nabla_x \ell(\theta_*(X_t^{1:N}), X_t^n) dt + \sqrt{2} dW_t^n \quad \forall n \in [N]. \quad (83)$$

As shown below, (83)'s law satisfies

$$\dot{q}_t(x^{1:N}) = -\nabla_{x^{1:N}} \cdot \left[ q_t(x^{1:N}) \nabla_{x^{1:N}} \log \left( \frac{\rho_N(x^{1:N})}{q_t(x^{1:N})} \right) \right], \quad (84)$$

where  $\rho_N$  is the (unnormalized) distribution on  $\mathcal{X}^N$  given by

$$\rho_N(x^{1:N}) := \prod_{n=1}^N p_{\theta_*(x^{1:N})}(x^n, y) \quad (85)$$

Clearly, the (unique) normalized fixed point of (84) (i.e. the stationary distribution of (83)) is

$$\pi_N(x^{1:N}) := \frac{\rho_N(x^{1:N})}{\mathcal{Z}_N} \quad \text{where} \quad \mathcal{Z}_N := \int \rho_N(x^{1:N}) dx^{1:N}. \quad (86)$$

As also shown below, (80,81)'s law satisfies

$$\begin{aligned} \dot{q}_t(\theta, x^{1:N}) = & -\nabla_\theta \cdot \left[ \frac{q_t(\theta, x^{1:N})}{N} \sum_{n=1}^N \nabla_\theta \ell(\theta, x^n) \right] \\ & - \nabla_{x^{1:N}} \cdot \left[ q_t(\theta, x^{1:N}) \nabla_{x^{1:N}} \log \left( \frac{\prod_{n=1}^N p_\theta(x^n, y)}{q_t(\theta, x^{1:N})} \right) \right], \end{aligned} \quad (87)$$

where, if necessary, the above should be interpreted weakly. Because  $\sum_{n=1}^N \nabla_\theta \ell(\theta_*(x^{1:N}), x^n) = 0$  by  $\theta_*(x^{1:N})$ 's definition, it is easy to check that

$$\pi_N(d\theta, dx^{1:N}) = \delta_{\theta_*(x^{1:N})}(d\theta) \pi_N(x^{1:N}) dx^{1:N}$$

is a fixed point of (87) (i.e. a stationary distribution of (80,81)). Similar manipulations show that the above is also a stationary distribution of (81,82). Our algorithms use the empirical distribution of the particles to approximate the posterior. Hence, for the estimates they produce to be ‘unbiased’, it would have to be the case that

$$\int \left( \theta_*(x^{1:N}), \frac{1}{N} \sum_{n=1}^N \delta_{x^n}(dx) \right) \pi_N(dx^{1:N}) = (\theta_*, p_{\theta_*}(dx|y)),$$

for some stationary point  $\theta_*$  of  $\theta \mapsto p_\theta(y)$ . However, because  $\theta_*(x^{1:N})$  is invariant to permutations of  $x^{1:N}$ 's components,  $\pi_N$ 's definition in (85,86) implies that its marginals  $\pi_N(dx^1), \dots, \pi_N(dx^N)$  all equal the same distribution,  $\mu_N$  on  $\mathcal{X}$ . Hence,

$$\begin{aligned} \int \left( \frac{1}{N} \sum_{n=1}^N \delta_{x^n}(dx) \right) \pi_N(dx^{1:N}) &= \frac{1}{N} \sum_{n=1}^N \int \delta_{x^n}(dx) \pi_N(dx^n) = \frac{1}{N} \sum_{n=1}^N \int \delta_{x^n}(dx) \mu_N(dx^n) \\ &= \frac{1}{N} \sum_{n=1}^N \int \mu_N(dx) = \mu_N(dx). \end{aligned}$$

In summary, for our algorithms to yield unbiased estimates, it would need to be the case that

$$\left( \int \theta_*(x^{1:N}) \pi_N(dx^{1:N}), \mu_N(dx) \right) = (\theta_*, p_{\theta_*}(dx|y)).$$

It is easy to find examples in which the above fails to hold (see, for instance, App. H.1).

*Proof of (84).* (83)'s Fokker-Planck equation (e.g. [13]) reads

$$\dot{q}_t(x^{1:N}) = - \sum_{n=1}^N \nabla_{x^n} \cdot [q_t(x^{1:N}) \nabla_{x^n} \ell(\theta_*(x^{1:N}), x^n)] + \sum_{n=1}^N \nabla_{x^n} \cdot \nabla_{x^n} q_t(x^{1:N}). \quad (88)$$

But

$$-\nabla_{x^{1:N}} \cdot \left[ q_t(x^{1:N}) \nabla_{x^{1:N}} \log \left( \frac{\rho_N(x^{1:N})}{q_t(x^{1:N})} \right) \right] = - \sum_{n=1}^N \nabla_{x^n} \cdot \left[ q_t(x^{1:N}) \nabla_{x^n} \log \left( \frac{\rho_N(x^{1:N})}{q_t(x^{1:N})} \right) \right], \quad (89)$$

and, using  $\rho_N(x^{1:N})$ 's definition in (85),

$$\begin{aligned} \nabla_{x^n} \log \left( \frac{\rho_N(x^{1:N})}{q_t(x^{1:N})} \right) &= \nabla_{x^n} \log(\rho_N(x^{1:N})) - \nabla_{x^n} \log(q_t(x^{1:N})) \\ &= \nabla_{x^n} \ell(\theta_*(x^{1:N}), x^n) + \sum_{m=1}^N \nabla_\theta \ell(\theta_*(x^{1:N}), x^m) \cdot \nabla_{x^m} \theta_*(x^{1:N}) \\ &\quad - \frac{\nabla_{x^n} q_t(x^{1:N})}{q_t(x^{1:N})}. \end{aligned} \quad (90)$$

But,  $\theta_*(x^{1:N})$ 's definition implies that

$$\nabla_{x^1} \theta_*(x^{1:N}) = \dots = \nabla_{x^N} \theta_*(x^{1:N}), \quad \sum_{m=1}^N \nabla_{\theta} \ell(\theta_*(x^{1:N}), x^m) = 0.$$

Hence, the middle term in (90)'s RHS equals zero and (84) follows from (88,89).  $\square$

*Proof of (87).* This is straightforward: (80,81)'s Fokker-Planck equation (e.g. [13]) reads

$$\begin{aligned} \dot{q}_t(\theta, x^{1:N}) &= -\nabla_{\theta} \cdot \left[ \frac{q_t(\theta, x^{1:N})}{N} \sum_{n=1}^N \nabla_{\theta} \ell(\theta, x^n) \right] - \sum_{n=1}^N \nabla_{x^n} \cdot [q_t(\theta, x^{1:N}) \nabla_{x^n} \ell(\theta, x^n)] \\ &\quad + \sum_{n=1}^N \nabla_{x^n} \cdot \nabla_{x^n} q_t(\theta, x^{1:N}). \end{aligned}$$

But,

$$\begin{aligned} &\nabla_{x^{1:N}} \cdot \left[ q_t(\theta, x^{1:N}) \nabla_{x^{1:N}} \log \left( \frac{\prod_{n=1}^N p_{\theta}(x^n, y)}{q_t(\theta, x^{1:N})} \right) \right] \\ &= \sum_{n=1}^N \nabla_{x^n} \cdot \left[ q_t(\theta, x^{1:N}) \nabla_{x^n} \log \left( \frac{\prod_{n=1}^N p_{\theta}(x^n, y)}{q_t(\theta, x^{1:N})} \right) \right] \\ &= \sum_{n=1}^N \nabla_{x^n} \cdot \left[ q_t(\theta, x^{1:N}) \left( \nabla_{x^n} \ell(\theta, x^n) - \frac{\nabla_{x^n} q_t(\theta, x^{1:N})}{q_t(\theta, x^{1:N})} \right) \right] \\ &= \sum_{n=1}^N \nabla_{x^n} \cdot [q_t(\theta, x^{1:N}) \nabla_{x^n} \ell(\theta, x^n)] + \sum_{n=1}^N \nabla_{x^n} \cdot \nabla_{x^n} q_t(\theta, x^{1:N}). \end{aligned}$$

$\square$

## H.1 Continuum limits for Ex. 1

By (51) and  $\rho_N$ 's definition in (85),

$$\begin{aligned} \rho_N(x^{1:N}) &= \prod_{n=1}^N \exp \left( -\frac{1}{2} \|y - x^n\|^2 - \frac{1}{2} \left\| x^n - \frac{\mathbf{1}_{ND_x}^T x^{1:N}}{ND_x} \mathbf{1}_{D_x} \right\|^2 \right) \\ &= \exp \left( -\frac{1}{2} \|y^{1:N} - x^{1:N}\|^2 - \frac{1}{2} \left\| x^{1:N} - \frac{\mathbf{1}_{ND_x}^T x^{1:N}}{ND_x} \mathbf{1}_{ND_x} \right\|^2 \right), \end{aligned}$$

where  $y^{1:N}$  stacks  $N$  copies of  $y$ . Applying the expressions in [6, p. 92] and the Sherman–Morrison formula, we find that

$$\pi_N(x^{1:N}) = \frac{\rho_N(x^{1:N})}{\int \rho_N(x^{1:N}) dx^{1:N}} = \mathcal{N} \left( x^{1:N}; \frac{1}{2} \left( y^N + \frac{\mathbf{1}_{D_x}^T y}{D_x} \mathbf{1}_{ND_x} \right), \frac{1}{2} \left( I_{ND_x} + \frac{\mathbf{1}_{ND_x} \mathbf{1}_{ND_x}^T}{ND_x} \right) \right);$$

whose marginals are equal to

$$\mu_N(x) = \mathcal{N} \left( x; \frac{1}{2} \left( y + \frac{\mathbf{1}_{D_x}^T y}{D_x} \mathbf{1} \right), \frac{1}{2} \left( I_{D_x} + \frac{\mathbf{1}_{D_x} \mathbf{1}_{D_x}^T}{ND_x} \right) \right).$$

Comparing with (48), we see that the covariance matrix is slightly off with a  $\mathcal{O}(N^{-1})$  error. However, due to the linearity in the model, there is no bias in the  $\theta$  estimates:

$$\begin{aligned} \int \theta_*(x^{1:N}) \pi_N(x^{1:N}) dx^{1:N} &= \frac{\mathbf{1}_{ND_x}^T \int x^{1:N} \pi_N(x^{1:N}) dx^{1:N}}{ND_x} \\ &= \frac{1}{2ND_x} \left( \mathbf{1}_{ND_x}^T y^N + \frac{\mathbf{1}_{ND_x}^T \mathbf{1}_{ND_x} \mathbf{1}_{D_x}^T y}{D_x} \right) = \frac{\mathbf{1}_{D_x}^T y}{D_x} = \theta_*. \end{aligned}$$

## I Metropolis-Hastings methods

As mentioned at the end of App. G, one fairly obvious way to try to remove the bias (B1, Sec. 3) from the estimates produced by PGA, PQN, and PMGA is to replace the ULA kernels with ‘exact’ kernels whose stationary distributions coincide with the posteriors (e.g. by adding an accept-reject step to each individual particle update). Here, we consider other, slightly less obvious and (to the best of our knowledge) novel, extensions of the Metropolis-Hastings algorithm (e.g. [2]) that also tackle (S1,2, Sec. 1). While these methods need not necessarily be associated with an optimization routine, their comprehension is also aided by viewing (S1,2) as a joint problem over  $\theta$  and  $q$ . The methods have one practical downside that limits their scalability: similarly as with standard Metropolis-Hastings algorithms (e.g. see [5, 65, 39, 40] and references therein), the acceptance probability degenerates with increasing latent variable dimensions  $D_x$  and the particle numbers  $N$ . This, in turn, forces us to choose small step sizes  $h$  for large  $D_x$  and  $N$ , which leads to slow convergence. This is the reason why we focused on the ‘unadjusted’ methods in the main text, rather than the Metropolized ones in this appendix.

### I.1 Marginal variants

Suppose that Assumpt. 2 holds and, for the sake of discussion, that the marginal likelihood  $\theta \mapsto p_\theta(y)$  has a unique maximizer  $\theta_*$ . Notice that the entire particle system  $(X_k^{1:N})_{k=0}^\infty := (X_k^1, \dots, X_k^N)_{k=0}^\infty$  generated by PMGA (15) is a Markov chain taking values in  $\mathcal{X}^N$ . Its kernel is given by

$$K_N(x^{1:N}, z^{1:N}) := \prod_{n=1}^N K_{\theta_*(x^{1:N})}(x^n, z^n),$$

where  $K_\theta$  denotes the ULA kernel in (72). (The precise form of  $K_\theta$  is immaterial to the ensuing discussion as long as, for each  $\theta$ ,  $K_\theta$  is a Markov kernel on  $\mathcal{X}$ .) Ideally,  $K_N$ ’s stationary distribution would be  $\prod_{n=1}^N p_{\theta_*}(x^n|y)$  but (B1,2, Sec. 3) precludes it. Correcting for this using an accept-reject step requires evaluating  $\prod_{n=1}^N p_{\theta_*}(x^n, y)$ , which we cannot do because  $\theta_*$  is unknown. We can, however, evaluate  $\rho_N(x^{1:N})$  in (85) and instead add an accept-reject step with acceptance probability

$$a_N(x^{1:N}, z^{1:N}) := 1 \wedge \left( \frac{\rho_N(z^{1:N}) K_N(z^{1:N}, x^{1:N})}{\rho_N(x^{1:N}) K_N(x^{1:N}, z^{1:N})} \right). \quad (91)$$

Running Alg. 1, we then obtain a chain  $(X_k^{1:N})_{k=0}^\infty$  whose stationary distribution is given by  $\rho_N(x^{1:N})$ ’s normalization,  $\pi_N(x^{1:N})$  in (86). Under Assumpt. 2,  $\pi_N(x^{1:N})$  is the unique fixed point of the continuum limits of PGA, PQN, and PMGA, see App. H. In other words, by imposing the accept-reject step, we have removed the (B1, Sec. 3) source of bias (see Fig. 2c).

The other source (B2, Sec. 3) due to the finite population size remains, but it can be mitigated by growing  $N$ . In particular, by its definition,  $\theta_*(x^{1:N})$  is invariant to permutations  $x^{1:N}$ ’s components. Hence, the components of any vector  $(X^1, \dots, X^N)$  drawn from  $\pi_N$  are exchangeable (similarly for  $(X_k^1, \dots, X_k^N)$  in Alg. 1). By chaos (e.g. [13, 33]), we expect that, under appropriate technical conditions, there exists a distribution  $\pi$  in  $\mathcal{P}(\mathcal{X})$  to which all of  $\pi_N$ ’s marginals converge. It should follow that, under  $\pi_N$ ,

$$\frac{1}{N} \sum_{n=1}^N \delta_{x^n} \approx \pi \quad \Rightarrow \quad \theta_*(x^{1:N}) = \theta_* \left( \frac{1}{N} \sum_{n=1}^N \delta_{x^n} \right) \approx \theta_*(\pi),$$

---

**Algorithm 1** The marginal MH method.

---

```

1: Initial conditions:  $X_0^{1:N} := (X_0^1, \dots, X_0^N)$ .
2: for  $k = 0, \dots, K - 1$  do
3:   Propose: draw  $Z^{1:N} = (Z^1, \dots, Z^N)$  from  $K_N$ .
4:   Generate uniform R.V.: draw  $U_k$  from the uniform distribution on  $[0, 1]$ .
5:   if  $U_k \leq a(X_k^{1:N}, Z^{1:N})$ , with  $a(\cdot, \cdot)$  as in (91) then
6:     Accept: set  $X_{k+1}^{1:N} := Z^{1:N}$ .
7:   else
8:     Reject: set  $X_{k+1}^{1:N} := X_k^{1:N}$ .
9:   end if
10: end for

```

---

with the above holding exactly in the  $N \rightarrow \infty$  limit. Marginalising (85,86) and taking limits we would then find that  $\pi(x) \propto p_{\theta_*(\pi)}(x, y)$ . In other words,  $\pi$  satisfies the first order optimality condition for  $F_*$  in Sec. 2.3:  $\nabla F_*(\pi) = 0$ . It then follows from  $\theta_*(q)$ 's definition and Thrm. 3, that  $\theta_*(\pi)$  is a stationary point of  $\theta \mapsto p_\theta(y)$  and  $\pi$  is the corresponding posterior  $p_{\theta_*(\pi)}(\cdot|y)$ . While we yet lack rigorous statements formalizing this discussion, it is easy to verify that it holds true for analytically tractable models (e.g. App. H.1), and our numerical experiments seem to further corroborate it (e.g. Fig. 2c).

## I.2 Joint variants

We can also mitigate (B1, Sec. 3) for PGA and PQN (Secs. 2.1, 2.2) using a population-wide accept-reject step along the lines of that in App. I.1. To begin, note that these algorithms are special instances of

$$\theta_{k+1} = u(\theta_k, q_k^N) \quad \text{with} \quad q_k^N := \frac{1}{N} \sum_{n=1}^N \delta_{X_k^n}, \quad (92)$$

$$X_{k+1}^{1:N} \sim K_N^{\theta_k}(X_k^{1:N}, \cdot) \quad \text{with} \quad K_N^{\theta}(x^{1:N}, z^{1:N}) := \prod_{n=1}^N K_\theta(x^n, z^n), \quad (93)$$

where  $K_\theta$  denotes a Markov kernel on  $\mathcal{X}$  for each  $\theta$  in  $\Theta$  (in particular, the ULA kernel in (72), but this is once again unimportant) and  $u$  denotes an update operator satisfying (70). Clearly,  $(\theta_k, X_k^1, \dots, X_k^N)_{k=0}^\infty$  forms a Markov chain with transition kernel

$$K_N((\theta, x^{1:N}), (d\psi, dz^{1:N})) = \delta_{u(\theta, \bar{\delta}_{x^{1:N}})}(d\psi) K_N^\theta(x^{1:N}, dz^{1:N}) \quad \text{where} \quad \bar{\delta}_{x^{1:N}} := \frac{1}{N} \sum_{n=1}^N \delta_{x^n}.$$

Emulating our steps in App. I.1, we impose an accept-reject step with acceptance probability

$$a_N((x^{1:N}, \theta), (z^{1:N}, \psi)) := 1 \wedge \left( \frac{K_N^\psi(z^{1:N}, x^{1:N})}{K_N^\theta(x^{1:N}, z^{1:N})} \prod_{n=1}^N \frac{p_\psi(z^n, y)}{p_\theta(x^n, y)} \right), \quad (94)$$

so obtaining Alg. 2.

We have so far failed to obtain analytical expressions for the resulting chain's stationary distributions. However, it is straightforward to find heuristic arguments suggesting that, as  $N \rightarrow \infty$ , the  $(\theta, x^n)$ -marginal, for any  $n$ , of these distributions approaches measures of the form  $\delta_{\theta_*}(d\theta) p_{\theta_*}(x^n|y) dx^n$ , where  $\theta_*$  is a stationary point of the marginal likelihood. In particular, note that the i.i.d. structure in  $K_N^\theta$ 's definition ensures that the particle system is exchangeable (hence,  $X_k^1, \dots, X_k^N$  all have the same law  $q_k$ ). By propagation of chaos (e.g. see [13]), it is reasonable to expect that, for large  $N$ , the particle's empirical distribution,  $q_k^N$  in (92), closely approximates  $q_k$ :

$$q_k^N \approx q_k.$$

Suppose that the above holds exactly, and consider the resulting 'idealized version'  $(\tilde{\theta}_k, \tilde{X}_k^{1:N})$  of the chain  $(\theta_k, X_k^{1:N})$  produced by Alg. 2: just as in (92,93), except that the empirical distribution  $q_k^N$  in (92) is replaced

---

**Algorithm 2** The joint MH method.

---

```

1: Initial conditions:  $\theta_0$  and  $X_0^{1:N} := (X_0^1, \dots, X_0^N)$ .
2: for  $k = 0, \dots, K - 1$  do
3:   Propose: set  $\psi := u\left(\theta_k, N^{-1} \sum_{n=1}^N \delta_{X_k^n}\right)$  and draw  $Z^{1:N}$  from  $K_N^{\theta_k}$ .
4:   Generate uniform R.V.: draw  $U_k$  independently from the uniform distribution on  $[0, 1]$ .
5:   if  $U_k \leq a((\theta_k, X_k^{1:N}), (\psi, Z^{1:N}))$ , with  $a(\cdot, \cdot)$  as in (94) then
6:     Accept: set  $\theta_{k+1} := \psi$  and  $X_{k+1}^{1:N} := Z^{1:N}$ .
7:   else
8:     Reject: set  $\theta_{k+1} := \theta_k$  and  $X_{k+1}^{1:N} := X_k^{1:N}$ .
9:   end if
10: end for

```

---

by the exact law  $q_k$ . The idealized chain's one-dimensional law  $\mu_k(d\theta, dx^{1:N})$  satisfies

$$\mu_{k+1}(d\psi, dz^{1:N}) = \int \mu_k(d\theta, dx^{1:N}) P_N^{q_k}((\theta, x^{1:N}), (d\psi, dz^{1:N})), \quad (95)$$

where the ‘idealized kernel’  $P_N^q$  is given by

$$\begin{aligned} P_N^q((\theta, x^{1:N}), (d\psi, dz^{1:N})) &= a_N((\theta, x^{1:N}), (\psi, z^{1:N})) \delta_{u(\theta, q)}(d\psi) K_N^\theta(x^{1:N}, z^{1:N}) dz^{1:N} \\ &\quad + [1 - a((\theta, x^{1:N}), (\psi, z^{1:N}))] \delta_\theta(d\psi) \delta_{x^{1:N}}(dz^{1:N}). \end{aligned}$$

It is then straightforward to show that, for any stationary point  $\theta_*$  of the marginal likelihood,

$$\pi_N^*(d\theta, dx) := \delta_{\theta_*}(d\theta) \prod_{n=1}^N p_{\theta_*}(x^n | y) dx^n$$

is a stationary distribution of the idealized chain in the sense that

$$(\tilde{\theta}_0, \tilde{X}_0^{1:N}) \sim \pi_N^* \quad \Rightarrow \quad (\tilde{\theta}_k, \tilde{X}_k^{1:N}) \sim \pi_N^* \quad \forall k = 1, 2, \dots \quad (96)$$

In particular, detailed balance holds: for any  $(\theta, x^{1:N}) \neq (\psi, z^{1:N})$  satisfying

$$\begin{aligned} K_N^\psi(z^{1:N}, x^{1:N}) \prod_{n=1}^N p_\psi(z^n, y) &\leq K_N^\theta(x^{1:N}, z^{1:N}) \prod_{n=1}^N p_\theta(x^n, y), \\ \Rightarrow a_N((\theta, x^{1:N}), (\psi, z^{1:N})) &= \frac{K_N^\psi(z^{1:N}, x^{1:N})}{K_N^\theta(x^{1:N}, z^{1:N})} \prod_{n=1}^N \frac{p_\psi(z^n, y)}{p_\theta(x^n, y)}, \quad a_N((\psi, z^{1:N}), (\theta, x^{1:N})) = 1, \end{aligned} \quad (97)$$



we have that, with  $\pi_*(\cdot) := p_{\theta_*}(\cdot|y)$ ,

$$\begin{aligned}
& \pi_N^*(d\theta, dx^{1:N}) P_N^{\pi_*}((\theta, x^{1:N}), (d\psi, dz^{1:N})) \\
&= \delta_{\theta_*}(d\theta) \left( \prod_{n=1}^N p_{\theta_*}(x^n|y) \right) a_N((\theta, x^{1:N}), (\psi, z^{1:N})) \delta_{u(\theta, \pi_*)}(d\psi) K_N^\theta(x^{1:N}, z^{1:N}) dx^{1:N} dz^{1:N} \\
&= \delta_{\theta_*}(d\theta) \left( \prod_{n=1}^N p_{\theta_*}(x^n|y) \frac{p_\psi(z^n, y)}{p_\theta(x^n, y)} \right) \delta_{u(\theta, \pi_*)}(d\psi) K_N^\psi(z^{1:N}, x^{1:N}) dx^{1:N} dz^{1:N} \\
&= \delta_{\theta_*}(d\theta) \left( \prod_{n=1}^N p_{\theta_*}(x^n|y) \frac{p_\psi(z^n, y)}{p_{\theta_*}(x^n, y)} \right) \delta_{u(\theta_*, \pi_*)}(d\psi) K_N^\psi(z^{1:N}, x^{1:N}) dx^{1:N} dz^{1:N} \\
&= \delta_{u(\theta_*, \pi_*)}(d\theta) \left( \prod_{n=1}^N \frac{p_{\theta_*}(z^n, y)}{p_{\theta_*}(y)} \right) \delta_{\theta_*}(d\psi) K_N^\psi(z^{1:N}, x^{1:N}) dx^{1:N} dz^{1:N} \\
&= \delta_{u(\psi, \pi_*)}(d\theta) \left( \prod_{n=1}^N p_{\theta_*}(z^n|y) \right) \delta_{\theta_*}(d\psi) K_N^\psi(z^{1:N}, x^{1:N}) dx^{1:N} dz^{1:N} \\
&= \delta_{u(\psi, \pi_*)}(d\theta) \left( \prod_{n=1}^N p_{\theta_*}(z^n|y) \right) a_N((\psi, z^{1:N}), (\theta, x^{1:N})) \delta_{\theta_*}(d\psi) K_N^\psi(z^{1:N}, x^{1:N}) dx^{1:N} dz^{1:N} \\
&= \pi_N^*(d\psi, dz^{1:N}) P_N^{\pi_*}((\psi, z^{1:N}), (d\theta, dx^{1:N})).
\end{aligned}$$

Reversing the roles of  $(\theta, x^{1:N})$  and  $(\psi, z^{1:N})$ , we find that the above also holds should the inequality (97) be reversed. Because it holds trivially if  $(\theta, x^{1:N}) = (\psi, z^{1:N})$ , integrating both sides over  $(\theta, x^{1:N})$ , we find that

$$\int \pi_N^*(d\theta, dx^{1:N}) P_N^{\pi_*}((\theta, x^{1:N}), (d\psi, dz^{1:N})) = \pi_N^*(d\psi, dz^{1:N});$$

and (96) follows from (95).